2020-01-01

An Analysis and Representation in an Atlas Reference Space of Putative Appositions from Neurons Expressing Alpha-Melanocyte-Stimulating Hormone With Neurons Expressing Hypocretin/Orexin or Melanin-Concentrating Hormone

Vanessa Inez Navarro
University of Texas at El Paso

AN ANALYSIS AND REPRESENTATION IN AN ATLAS REFERENCE SPACE OF PUTATIVE APPOSITIONS FROM NEURONS EXPRESSING ALPHA-MELANOCYTE-STIMULATING HORMONE WITH NEURONS EXPRESSING HYPOCRETIN/OREXIN OR MELANIN-CONCENTRATING HORMONE

VANESSA I. NAVARRO

Master's Program in Biological Sciences

APPROVED:

_____
Arshad M. Khan, Ph.D., Chair

_____
Hugues Ouellet, Ph.D.

_____
Vanessa Routh, Ph.D.

_____
Stephen Crites, Ph.D.
Dean of the Graduate School

AN ANALYSIS AND REPRESENTATION IN AN ATLAS REFERENCE SPACE OF PUTATIVE APPOSITIONS FROM NEURONS EXPRESSING ALPHA-MELANOCYTE-STIMULATING HORMONE WITH NEURONS EXPRESSING HYPOCRETIN/OREXIN OR MELANIN-CONCENTRATING HORMONE

by

Vanessa I. Navarro, B.S.

THESIS

Presented to the Faculty of the Graduate School of

The University of Texas at El Paso

in Partial Fulfillment

of the Requirements

for the Degree of

MASTER OF SCIENCE

Department of Biological Science

THE UNIVERSITY OF TEXAS AT EL PASO

August 2020

Acknowledgments

I would like to thank my committee members, Dr. Vanessa Routh and Dr. Hugues Ouellet, for their time and support for my thesis. Also, thank you to the lab members of the UTEP Systems Neuroscience Laboratory. My special thanks goes to Dr. Christina D'Arcy and Kenichiro Negishi for their helpful discussions, guidance, and support through everything. Thank you to Eduardo Peru for the incredible support and patience through this journey; having you by my side made everything better. Thank you for never giving up on me. To my PERSIST students, Josdell Guerra, Andrea Guevara, and Lidice Soto, thank you for the long hours of hard work mapping and working at the microscope. Alejandro Toccoli and Diana Sotelo, thank you for allowing Eddie and me to be your graduate mentors. Thank you for staying with us during long nights mapping, taking pictures, counting cells, creating posters and, more importantly, for the many laughs and awesome experiences through it all. Most importantly, thank you both for being our friends. None of the work presented in this study would have been possible without the help and dedication of the students. I would also like to thank my mother Clara and sister Claudia for their unconditional love and support through every step of this journey. You both are my inspiration, my rock, my everything. Finally, I am incredible thankful for the support, professional development, advice, and guidance from Dr. Arshad Khan. Thank you for allowing me to be part of this crazy ride.

Abstract

The hypothalamus is a brain structure at the center of a variety of regulatory functions that have been explored by scientists and clinicians for almost a century. Among these functions, metabolic regulation and the control of appetitive behaviors have been fields of intensive research. Some of the major neural substrates involved in the hypothalamic control of feeding and the regulation of metabolic state include neuronal populations that express the neuropeptides alpha-melanocyte stimulating hormone (αMSH), melanin-concentrating hormone (MCH) and hypocretin/orexin (H/O). αMSH has been characterized in part as an anorexigenic peptide, while MCH and H/O have been characterized as having orexigenic effects. The functionally opposing nature of these neuropeptides has prompted researchers to investigate the effects that αMSH might have in modulating H/O and MCH actions, which has uncovered structural evidence of putative appositions between axonal fibers from hypothalamic cells expressing αMSH and cell bodies, or somata, of other hypothalamic cells expressing either H/O or MCH. However, these groups did not report their findings within a standardized spatial framework, nor did they provide detailed co-spatial distributions – for the regions of possible synaptic interactions – for these neuropeptides. In the present study, immunohistochemical staining and rigorous atlas-based mapping were used to pinpoint the distributions of αMSH-, MCH- and H/O-immunoreactive somata and fibers throughout the anterior, and tuberal hypothalamus in order to determine regions with a high likelihood of local interactions or co-spatial expression. Additionally, at a finer scale, these methods were employed to report with high-spatial resolution the distributions of possible synaptic interactions of αMSH-ir fibers with either MCH- or H/O-ir somata. Collectively, these data will allow for more quantitative hypothesis-testing to determine whether there is a clear pattern or organization of the distributions of these neuropeptides and their structural interactions.

Table of Contents

List of Tables

List of Figures

Chapter I: Introduction

The location and organization of the hypothalamus makes it an ideal brain structure for the integration of information received by the central nervous system and the periphery (Simerly 2015, Schwartz et al 2000). Therefore, it is also an ideal structure for mediating behaviors and regulatory functions that are essential for survival. These include feeding, wakefulness, fluid balance, thermoregulation, sexual behaviors, reproduction, as well as the stress response and aggression (Saper and Lowell 2014). In order for the hypothalamus to perform these functions, it has neurons that are specialized to interact with signals coming from the periphery, which are in the form of hormones or levels of circulating molecules which directly are measure of some aspect of internal state (i.e., glucose, lipids, amino acids, osmolytes, temperature) (Routh et al 2014, Saper and Lowell 2014, Schwartz et al 2000, Siemens and Kamm 2018). Additionally, the hypothalamus receives inputs from regions that have processed sensory information and is believed to contextualize the signals being received from the periphery in order to produce adequate physiological responses to the information it is integrating (Dampney 2011; Saper and Lowell 2014).

Due to the integrative role of the hypothalamus in these essential responses, there has been strong research interest in defining its afferent and efferent connections. These efforts have demonstrated that hypothalamic regions receive hindbrain-originating afferents which provide direct sensory information, as in the case of thermoregulation, and also receive afferents from limbic regions such as the amygdala, cingulate cortex, and hippocampus; which can add salience and pathway-specific importance to the signals being processed by the hypothalamus in order to produce emotional responses based on physiological cues (Saper and Lowell 2014). These

incoming signals are processed and then ultimately result in the generation of efferent signals that can elicit either hormonal or vagal responses through the pituitary gland or through hindbrain projections.

However, information coming to and from the hypothalamus through these connections is not the complete story. Intrahypothalamic signaling is essential for processing the information coming to the hypothalamus and generating the appropriate output. Despite the critical importance of such signaling, the neuroanatomical organization underlying the neural coding that integrates hypothalamic signals is poorly understood. The functional diversity of the hypothalamus suggests that circuitry for these responses share common anatomical space, creating to some extent a need to parse out these anatomical connections within the context of each behavioral and autonomic response. In order to provide context about the importance of the anatomical aspects of this study, the next sections will expand on the anatomy and functional importance of three feeding-related neuropeptides found to be expressed in the hypothalamus, beginning first with alpha-melanocyte-stimulating hormone (αMSH), which is a part of the larger melanocortin neuropeptide system.

I.1. Melanocortins

The melanocortin family of peptides refers to those peptides generated when pro-opiomelanocortin (POMC) precursor protein is proteolytically processed by protein convertases (PCs) into a number of smaller polypeptide hormones (Chretien and Mbikay 2016). This family of peptides was the first reported to produce proteins with varying functions coming from the same precursor protein. These peptides include adrenocorticotropic hormone (ACTH), γ-lipotropin (γ-LPH) and β-lipotropin (β-LPH), corticotropin-like intermediate peptide (CLIP), β-melanocyte stimulating hormone (βMSH), γ-melanocyte stimulating hormone (γMSH) and αMSH (Chretien

and Mbikay 2016, Cone 2005). Long before it was known that αMSH was derived from POMC, this peptide had already been isolated from pig pituitary glands, when Dr. Aaron B. Lerner's group at Yale University School of Medicine did so in 1955. Two years later, the Lerner group published the amino acid sequence of αMSH. In 1979, Nakanishi and colleagues published the entire sequence of its precursor protein, ACTH-β-LPH precursor, which is now referred to as pro-opiomelanocortin (POMC). POMC-expressing neurons can be found in a variety of hypothalamic nuclei; however, a large portion of αMSH immunoreactive (αMSH-ir) somata can be found within the arcuate hypothalamic nucleus (ARH), with few somata crossing over into neighboring areas (Guy et al 1982, Kiss et al 1984, Jacobowitz et al 1978). αMSH-ir fibers, on the other hand, can be found throughout various regions of the brain; however, they are distributed in greater densities within the periventricular (PV), paraventricular (PVH) and dorsomedial hypothalamic (DMH) nuclei. The distribution and POMC origin of αMSH were known far before its physiological effects, which were not characterized until the 1980s, when central administration of this neuropeptide in different studies was reported to affect sexual behaviors and to suppress feeding. Receptors for the melanocortins vary in function and localization though out the body: MCR_1 has been observed to be present in leukocytes and play a role in mediating inflammation. MCR_2 mediates the effects of ACTH on steroid secretion. MCR_3 and MCR_4 are extensively found in the central nervous system, where MCR_3 has been linked to energy homeostasis and MCR_4 to food intake, among other functions. Finally, MCR_5 is expressed in human peripheral tissues and is involved in exocrine function (Yang, 2011). Since the 1980s, MCH has been found to play roles in increasing aggression and anxiety, and in attenuating inflammatory responses in the body (Star et al 1995, Rao et al 2003). However, within the nervous system, the major functional focus of research for this neuropeptide has been on its role as an anorexigenic neuropeptide.

I.2. Hypocretin/orexin

Hypocretin/orexin (H/O) is a neuropeptide that has two isoforms, referred to as hypocretins 1 and 2 (orexins A and B, respectively) which bind to two separate G-protein coupled receptors, Hcrtr1 and Hcrtr2 (Ox1R and Ox2R, respectively) (Marcus et al 2001). The discovery of the hypocretin/orexins was reported by two independent groups nearly simultaneously (Sakurai et al 1998, de Lecea et al 1998). In these initial descriptions, H/O-ir somata were found to be localized in the DMH and lateral hypothalamic area (LHA), which was confirmed by later studies (Swanson et al 2005, Hahn 2010). When administered intracerebroventricularly (icv) by the Sakurai group, H/O led to increased food intake, which was the first behavioral function known for H/O (Sakurai et al., 1998). Later studies determined that some of the effects that H/O has on feeding take place through the modulation of reward pathways by way of projections to VTA dopaminergic neurons in response to low glucose levels from fasting and weight loss (Borgland 2006, Sheng et al 2014, Teegala et al 2018). Although H/O-ir somata are restricted to LHA and neighboring regions, H/O-ir fibers were also observed throughout various regions of the brain including the locus coeruleus, the raphe nuclei, and the pontine reticular formation as well as various hypothalamic regions, such as the VMH, ARH, and PVH. The distribution of the receptors for H/O, as well as the axonal distribution of this neuropeptide, have implied roles for H/O that go beyond just feeding. Specifically, later studies demonstrated that, in addition to feeding, this neuropeptide plays a role in wakefulness, arousal, addiction and drinking behaviors.

I.3. Melanin-concentrating hormone

The discovery of melanin-concentrating hormone (MCH) in 1983 came about as an effort to find evidence for a peptide theory proposed by Hogben and Slome in 1931. This theory proposed

that the pigmentation of amphibian skin was regulated by antagonizing "agencies" later discovered to be the peptide neurotransmitters αMSH (lightening of the skin) and MCH (darkening of the skin) (Kawauchi et al 1983). MCH was found to come from a precursor protein, pro-melanin concentrating hormone (PMCH), which, when cleaved gives rise to MCH, neuropeptide- glutamic acid-isoleucine (NEI) as well as neuropeptide-glycine-glutamic acid (NGE) (Bird et al 1990). Its effects on skin pigmentation of fish were later found to be only one of many roles for this peptide that is highly conserved across species. It was found in 1996 that when MCH was administered intracerebroventricularly (icv) in rats, there was an increase in food consumption. Much like H/O, somata that are immunoreactive for MCH are found mostly in the LHA and neighboring regions in the rat. However, MCH-ir somata extend more dorsally into the zona incerta (ZI) and more caudally into the posterior hypothalamus (PH), with MCH-ir axons found throughout the entirety of the brain. The highest densities of MCH-ir axons have been reported in the cerebral cortex, thalamus, amygdala, hippocampus, septum, basal ganglia, the superior and inferior colliculi, parabrachial nucleus, periaqueductal grey, ventral tegmental area, raphe nuclei, interpeduncular nuclei, and reticular formation as well as within the hypothalamus (DMH, anterior hypothalamic nucleus (AHN), preoptic area, and LHA) (Nahon et al 1989, Bittencourt et al 1992, Swanson et al 2005, Hahn 2010). Much as with H/O, this widespread distribution of MCH-ir fibers throughout the brain led researchers to hypothesize a variety of functions for this neuropeptide, many of which overlap with the proposed and established functions of H/O. Although icv administration of MCH did elicit an increased food consumption in sated rats, and the expression of this neuropeptide was observed to increase with fasting (Qu et al 1996), there was no effect observed on normal body weight, indicating that MCH has a role in food intake control but not in the regulation of body weight (Rossi et al 1997). MCH has also been reported to affect behaviors such as drinking,

reproduction and sleeping, as well as the endocrine functions of both the hypothalamic-pituitary-adrenal axis and the hypothalamic-pituitary-thyroid axis.

I.4. Anatomy of the hypothalamus

The hypothalamus is subdivided into three mediolateral zones (periventricular, medial and lateral) containing different nuclei, each with their own connectional profiles (Simerly 2015). The medial zone nuclei, for the most part, are very well defined in terms of their cytoarchitectural organization, making their identification easier and more common in atlas representations (Simerly 2015). The lateral zone, however, has often been viewed as a large monolithic structure (e.g., in the atlases of Paxinos and Watson, Paxinos and Franklin, and the Allen Reference Atlas) and is usually not subdivided. The LHA, however, consists of different heterogeneous populations that have been subdivided into 16 provisional cytoarchitecturally-defined subdivisions by Swanson (2018). These subdivisions may become relevant when investigating the spatial distributions of neuronal populations within the LHA, such as MCH and H/O. Studies examining the neuronal activation of H/O-ir neurons have demonstrated that there are a larger number of activated H/O neurons when rats are emerging from sleep and this difference seems to be regionalized, as medial and perifornical H/O-expressing neurons were activated far more than those located more laterally (Estabrooke et al 2001). This regionalization of function was also demonstrated to extend to addiction, with subpopulations of H/O-expressing neurons projecting to ventral tegmental area (VTA). Specifically, caudal VTA-projecting H/O neurons were found to be involved in morphine-induced conditioned place preference in rats with dependence while rostral VTA-projecting H/O neurons were involved in condition place preference of non-dependent rats (Richardson and Aston-Jones 2012). These regional effects of function are not limited to H/O, but are also observed when examining the functions of MCH; for example, during activation in MCH neurons during

the induction of REM sleep. The distributions of activated MCH-expressing neurons during REM sleep also has a distinct regional distribution (Verret et al 2003). However, none of these aforementioned studies for either H/O or MCH use any type of reporting that would allow for these different datasets to be placed into the same spatial model for comparison across cases and for determining any patterns for these distributions that could become apparent from such a comparison.

This lack of common spatial framework has also been apparent in studies of the intrahypothalamic connections of feeding circuits. MCH, H/O and αMSH are neuropeptides which have demonstrated interactions within the hypothalamus which could be related to feeding and energy balance (Nahon et al 2006, Saper 2014). ARH αMSH-expressing neurons receive peripheral signals from the pancreas and adipose tissues in the form of insulin and leptin, respectively, which can lead to a decrease in feeding. These effects have been demonstrated to be mediated downstream, in part, by the neuropeptides, H/O and MCH (Nahon et al 2006). Previous studies have shown through the use of immunohistochemical stains that αMSH-ir fibers form putative appositions with both H/O- and MCH-expressing neurons in the hypothalamus (Elias et al 1998). Additional confirmation for these interactions came from follow-up studies which used genetically encoded tracers to demonstrate that H/O-expressing neurons receive inputs from αMSH-expressing neurons (Sakurai et al 2005). However, much like the functionally-defined distributions of H/O- and MCH-expressing neurons, these datasets for αMSH-ir interactions with these orexigenic peptides have not been mapped using atlas-based approaches. Therefore, since they cannot be brought into registration with other datasets, the spatial distributions of their interactions are difficult to compare at a sub-regional level within the hypothalamus. This could mean that the subtle intricacies of intrahypothalamic communication may be eluding us simply

because the experimental data provided in the literature has not been brought into a common spatial framework with enough precision to begin to see possible patterns that underlie such communication.

I.5. Specific Aims

Specific Aim 1: To conduct atlas-based mapping of H/O, MCH and αMSH in the hypothalamus using the Swanson reference atlas in order to determine novel patterns of co-spatial organization**.**

The distributions of αMSH, MCH and H/O neuropeptidergic signals have been extensively characterized in various studies. Some of these studies have even mapped these peptides using an atlas-based approach; however, there has not been an atlas-based analysis of these neuropeptide distributions in a systematic way across various cases or in relation to one another in the same brain. In the present study, the use of immunohistochemical stains for a combination of αMSH and H/O across three animal cases will be used in order to generate maps showing ***areas of high and low variability*** for the presence of immunoreactive fibers and somata throughout a major extent of the anterior, and tuberal divisions of the hypothalamus. We aim to provide maps of these distributions to help other researchers who use techniques that require the precise localization of neurons for investigation of synaptic interactions, as is the case with techniques such as like patch-clamp electrophysiology, electron microscopy and optogenetics/chemogenetics.

Specific Aim 2: To extend the predictive power of atlas-based mapping by identifying and mapping the distributions of putative αMSH-ir axonal appositions with H/O- or MCH-ir cell populations using the Swanson reference atlas**.**

Studies like those conducted by Elias et al 1998 and others have demonstrated the presence of putative appositions from αMSH-ir axonal fibers onto MCH- and H/O-ir cell bodies. These studies – although demonstrating the presence of these appositions – did not give the discerning reader a sense of the distributions or which regions display greater numbers of these sub-cellular elements. This would make investigating their interactions difficult, as this would require prior knowledge of locations where finding these possible synaptic interactions would be more likely. By conducting a regional analysis of putative appositions throughout the dorsoventral and mediolateral extents of the hypothalamus on an atlas-level basis, the aim here is to provide high-spatial resolution distributions for these possible interactions. By contextualizing these data using a common spatial framework, we are able to compare across different animal cases and provide zones of high consistency for putative interactions. The use of these methods will allow for the generation of the highest spatial resolution maps for distributions of these putative appositions, aiding in the future exploration of the interactions between these two cell populations.

Chapter II: Materials and Methods

II.1. Experimental subjects

Adult male Sprague Dawley rats (290–350 g body weight) were housed in a temperature and humidity-controlled vivarium with a 12 h:12 h light:dark photoperiod (lights on at 7:00 A.M.). Animals were given access to food and water *ad libitum*. All protocols were approved and sanctioned by the Institutional Animal Care and Use Committee of the University of Texas at El Paso.

II.2. Transcardial perfusion and tissue sectioning

Between four and six hours after the onset of the light cycle, animals were deeply anesthetized under 4% isoflurane (Vedco, St. Joseph, MO) in an induction chamber (Scienceware, South Wayne, WI) prior to transcardial perfusion with ice-cold 0.9% saline. This was followed by perfusion with 4% paraformaldehyde (PFA) dissolved in 0.05 M phosphate-buffered saline (PBS) (pH 7.4 at room temperature). Following fixation, brains were then carefully removed and placed in additional fixative solution (buffered 4% PFA), then stored in 0.05 M phosphate-buffered saline (PBS) with 20% sucrose for 24 hours at 4°C. The brains were then rapidly frozen in supercooled hexanes for long-term storage at –80°C. Prior to tissue sectioning, brains were blocked into hindbrain and forebrain in order to acquire only the sections of the tissue needed. The remaining blocked tissue was then frozen and stored at –80°C. Tissue was sectioned in the coronal plane at 30 μm thickness using a Reichert sliding microtome (Reichert, Austria, Nr. 15 156) fitted with a modified freezing-stage (Brain Research Laboratories, Newton, MA; Cat#3488-RJ). Tissue sections were collected as six 1-in-6 series and placed into 24-well plates filled with cryoprotectant solution (30% ethylene glycol, 20% glycerol in 0.05 M sodium phosphate buffer) for storage at –

20°C until further processing. The second tissue series collected was reserved for preparing a cytoarchitectural reference series using Nissl staining, with the remaining tissue series reserved for immunohistochemical analyses.

II.3. Histochemistry

II.3.1. Nissl Staining—Sections were removed from cryoprotectant solution and washed five times for a period of five minutes (5×5) in netted well trays with 0.05 M Tris Buffered Saline (TBS) solution (3.3% Tris HCl, 0.47% Tris OH in normal saline; pH 7.4 at room temperature) prior to mounting them onto gelatin-coated slides (Simmons and Swanson, 1993). Sections were allowed to air-dry overnight at room temperature prior to sequential dehydration in ascending ethanol concentrations (50%, 70%, 95%, and 3×100% for 3 min each) and delipidized in xylene for 25 min. Sequential rehydration of the sections was performed in descending ethanol concentrations (100%, 95%, 70% and 50% for 3 min each), and then rinsed with distilled water for 3 min prior to staining with 0.25% thionine for 1 min and 30 sec. The tissue sections were then immediately rinsed with distilled water and placed in 0.4% glacial acetic acid for 1 min to remove excess thionine and differentiate the areas. Stained tissues were again sequentially phased through progressively non-aqueous solvent solutions (50%, 70%, 95%, and 3 ×100% ethanol for 3 min each). Sections were later cleared with xylenes for 25 min and finally coverslipped with dibutylphthalate polystyrene xylene (DPX) mounting medium (catalog #06522; Sigma-Aldrich, St. Louis, MO).

II.3.2. Immunoperoxidase Histochemistry (IHC)— Immunoperoxidase staining was performed on a series of tissue sections adjacent to that of the Nissl-stained series. Sections were transferred in a netted washing tray filled with 0.05 M TBS (25°C, pH 7.4) for five washes of five minutes each

(5×5) in order to remove cryoprotectant. The netted tray containing the sections was then filled with a solution of TBS containing 0.014% phenylhydrazine, which was allowed to mix with sections for 20 min to suppress endogenous peroxidase activity. Sections were again washed 5×5 with TBS and placed in blocking solution (2% (v/v) normal donkey serum (EMD Millipore (now MilliporeSigma), Burlington, MA; Catalog #S30-100ML; Lot #2510142); 0.1% Triton X-100 (Sigma-Aldrich; Catalog #T8352-500ML, Lot #MKBH4307V); in TBS) to incubate for one hour. Sections were then transferred into a sterile 24-well plate containing primary antibody solution for 48–72 hours at 4°C (details outlined in **Table 1**). For the following procedure, biotin-conjugated secondary antibodies were separated into two staining rounds to allow for independent staining with 3, 3'-diaminobenzidine (DAB) (*brown signal*) (Sigma-Aldrich) and ammonium nickel (II) DAB (*dark purple signal*). Sections were washed 5×5 and transferred to their respective secondary antibody solutions containing biotinylated donkey-derived antibodies to incubate for 5 hours. Sections were then placed in 5×5 washes in TBS and then into avidin-biotin-horseradish peroxidase complex-containing solution (Vectastain Elite ABC-peroxidase kit, Vector Laboratories, Catalog #PK-6100, RRID:AB_2336819; 0.45% v/v reagents A and B; 0.1% Triton X-100 in 0.05 M TBS). Sections were then washed 5×5 and placed in their respective immunoperoxidase solutions containing 0.1% w/v ammonium nickel (II) sulfate, 0.05% 3, 3' diaminobenzidine, 0.005% (v/v) H_2O_2 and 0.05 M TBS, and then observed until an adequate signal was obtained. Steps for secondary staining were then repeated for the second antigen, except the DAB solution did not include ammonium nickel (II) (0.05% w/v DAB, 0.015% v/v H_2O_2 dissolved in 0.05 M TBS). A final 5×5 wash was performed, and then sections were mounted onto gelatin-coated slides and allowed to dry overnight at room temperature. Slides with mounted sections were then dehydrated in ascending concentrations of ethanol (50%, 70%, 95%, 100% for 3 minutes

each), followed by 25 minutes in mixed xylenes to defat the tissue. DPX (Catalog #06522; Sigma-Aldrich) mounting medium was then used to coverslip the slides.

Table 1. Reagents used for Immunohistochemistry

Reagent	Antigen/Conjugate	Host	Type	Source	Dilution	Incubation
Primary	Hypocretin I/Orexin A	Gt	polyclonal IgG	Santa Cruz	1:4,000	72 h, 4°C
	α-MSH	Sh	polyclonal IgG	Millipore	1:10,000	72 h, 4°C
	MCH	Rb	polyclonal IgG	Phoenix	1:10,000	72 h, 4°C
Secondary	anti-goat IgG	Dk	biotinylated	Jackson	1:500	5 h, RT
	anti-sheep IgG	Dk	biotinylated	Jackson	1:500	5 h, RT
	anti-rabbit IgG	Dk	biotinylated	Jackson	1:500	5 h, RT
Conjugate	Avidin	-	HRP-Conjugated (ABC kits)	Vector	1:1,000	1 h, RT
Chromagen	DAB Mixture	-	-	Sigma	See Footnote 1	Variable

1. Added to this was 1 mM Ammonium Nickel (II) Sulfate Hexahydrate (Sigma), 0.002% DAB (Sigma), and 0.005% H_2O_2 (Sigma)

II.4. Imaging and Image Alignment

II.4.1. Bright-field Imaging—An Olympus BX63 light microscope equipped with an DP74 color camera with X-Y-Z motorized stage (Olympus Corporation, Center Valley, PA) driven by cellSense™ Dimension software (Version 2.3) was used to image and stitch Nissl- and DAB-stained tissue sections. Hemi-sections corresponding to the same side of the brain for both sets of tissues were imaged at ×10 magnification (N.A.,0.3) for alignment purposes. Another set of photographs of DAB-stained tissues was obtained at ×100 magnification (N.A.,1.4) to demonstrate individual putative appositions. An Olympus BX53 light microscope (Olympus Corporation, Tokyo, Japan) was used to confirm and map the putative appositions for quantification. When necessary, Adobe Photoshop (in Adobe Creative Cloud; Version CC 18.0.0; Adobe Systems, Inc., San Jose, CA) was used to adjust the brightness and contrast of the photomicrographs, and then to later export the images as TIFF-formatted files.

II.4.2. Image Alignment and Demarcation—High-resolution images of bright-field immunoperoxidase-stained sections, along with images of a reference Nissl-stained adjacent tissue series, were imported into Adobe Illustrator (AI; Version CC 18.0.0; Adobe) as individual data layers and aligned with one another using white matter tracts and vascular features in the tissue sections to bring them into register, as described previously (Zséli et al., 2016). Images of Nissl-stained tissues were adjusted for brightness or contrast when not optimally stained. Other than rotation and scaling adjustments for alignment purposes, no other alterations were made for images of the immunoperoxidase-stained tissues. In some instances, the adjacent Nissl-stained tissue series was lost or too distorted to be faithfully aligned with its immunoperoxidase-stained tissue counterpart (**Figure 1**). Data layer overlays were created in AI in which the boundaries of gray and white matter regions for the reference images for Nissl-stained tissues were rendered and in which immunoreactive cell somata (denoted by *filled circles*) and fibers (marked by *solid lines*) were plotted for the antigens, αMSH, H/O, and MCH. Additional refinement of cell somata denotation was performed when analyzing tissue sections under ×100 magnification in order to increase accuracy of the cell counts in later steps.

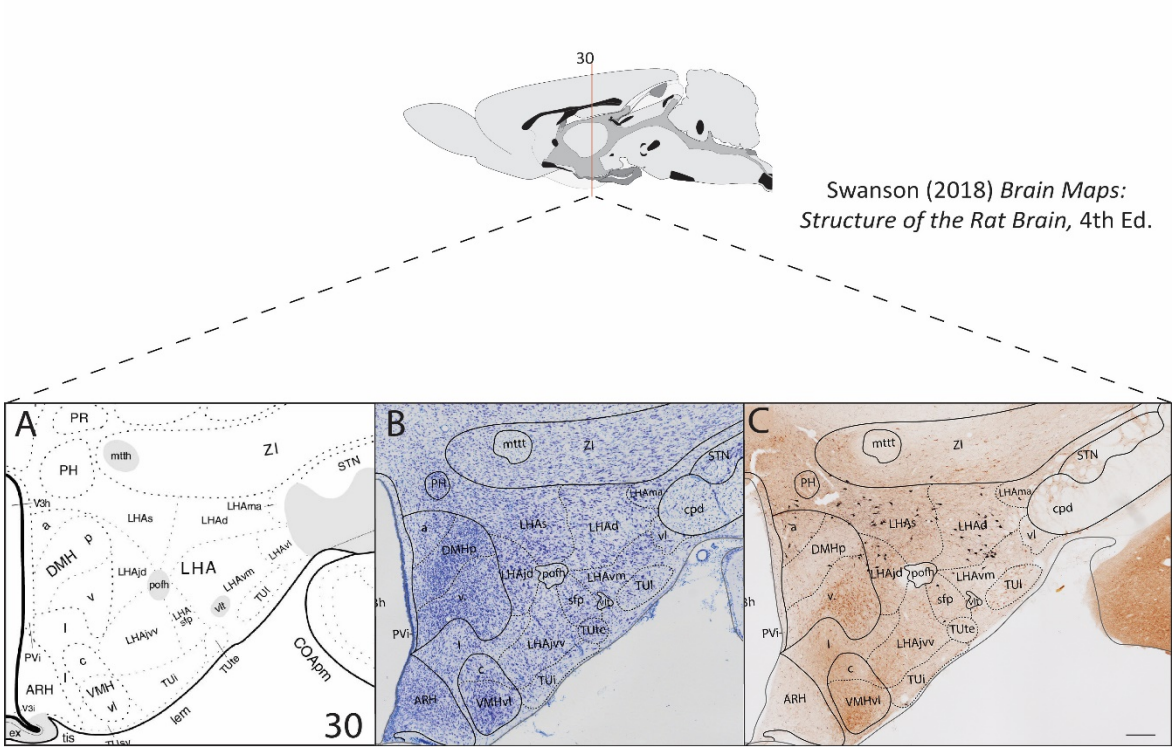

Figure 1. Schematic representation of the mapping process. From left to right, **(A)** an atlas template (Level 30) used to determine hypothalamic sub-regional boundaries on **(B)** Nissl-stained sections, based on cytoarchitectural analysis, which are then overlaid onto **(C)** an adjacent tissue series from the same animal which was immunoperoxidase-stained for relevant neuropeptides. Sections were overlaid using separate layers in Adobe Illustrator and aligned with the use of fiducial landmarks on both stained sections. Images were obtained at ×10 magnification and stitched using cellSense™ software. Please consult the Appendix for an explanation of the abbreviations used in this figure. Scale bar in **Panel C** represents 200 µm and also applies to **Panel B**

II.5. Analysis of Putative Appositions

Aligned Nissl and DAB files were used together as a guide to locate and observe each cell body under a microscope at ×100 magnification (N.A., 1.25) for putative appositions. Whenever a cell was identified to have a putative apposition, the color of the already mapped cell body would be changed. If a cell was checked and not found to contain a putative apposition, the color of the stroke would be changed to indicate that the cell had been analyzed. The following criteria were

used to determine all putative appositions (Krimer et al 1997, Lambe et al 2000): 1. Clearly identifiable cell body and fiber within the same focal plane;

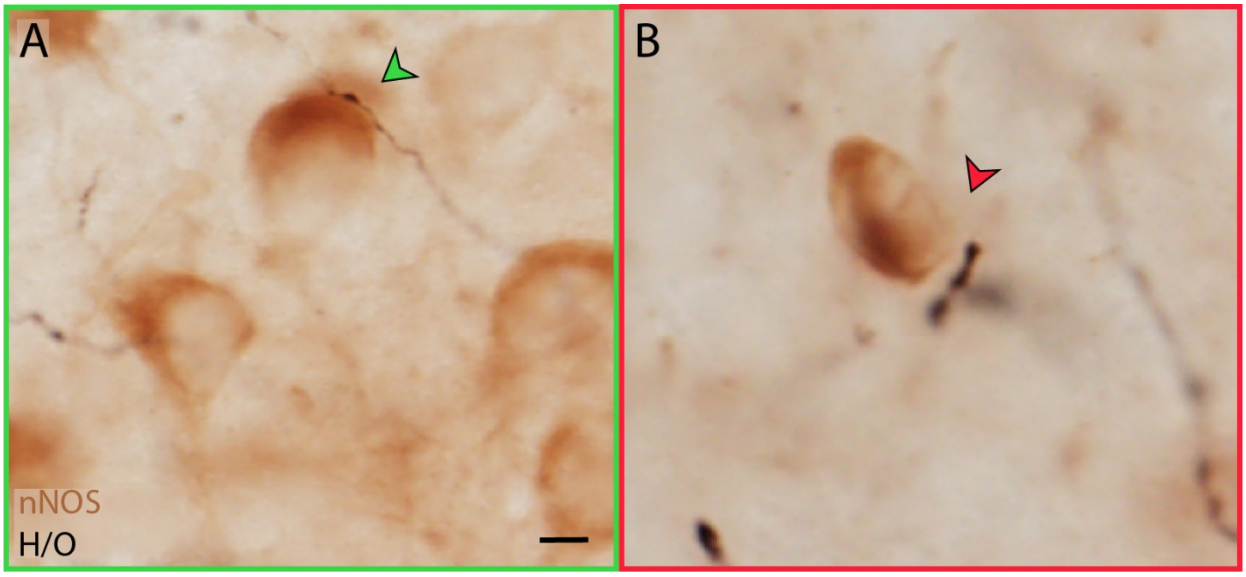

Figure 2. Examples of criteria for putative appositions. **A.** The green box shows an example of a positive putative apposition; an H/O-ir bouton is shown to be putatively contiguous with nNOS-ir cell body within the same focal plane. **B.** The red box demonstrates an example of a negative putative apposition; a space can be observed between an nNOS-ir cell body and H/O-ir boutons. Images obtained at ×100 magnification. Scale bar in **Panel A** represents 5 µm and also applies to **Panel B**.

---

2. No visible space observed between the fiber and cell body in any focal plane; and 3. The fiber can be followed in and out of focus as it contacts the cell body. (**Figure 2** shows an example of what is considered a putative apposition; for more examples, please see **Figures 6 and 8**).

II.5.1. Semi-quantitative analysis of cell counts—The total counts for cells containing putative appositions for each neuropeptide were acquired by sub-region using the *Lasso* and *Document Information* tools in Adobe Illustrator (Adobe Creative Cloud CS5) to count ellipses that had been used to mark the presence of each cell. Similarly, cell counts for each peptide were acquired and used to provide percentages of cells containing putative appositions with respect to the total

number of cells by region. The analysis of cell bodies in this study is semi-quantitative, and therefore, provides an assessment of the number of cells observed rather than a full representation of each region (see **Figures 7 and 9** for maps of putative appositions).

II.6. Translation of Data to the Atlas

Data from direct image overlays were translated to the Swanson rat brain atlas (*Brain Maps 4.0*; Swanson, 2018) using an approach as previously described (Zséli et al., 2016). Briefly, the distributions of cells and fibers were examined in the context of orientation (fiber direction) and positional relationship to the experimental tissue's regional boundaries. Adjustments to accommodate regional distortions between the experimental tissue and the atlas representation were approximated and applied to the data, being careful to preserve the relative distributions and orientations of the labeled elements.

Chapter III: Results

III.1. Aim 1: To conduct atlas-based mapping of H/O, MCH and αMSH in the hypothalamus using the Swanson reference atlas in order to determine novel patterns of co-spatial organization.

In order to determine the spatial distributions of the data plotted in the maps generated in this study, cytoarchitectural criteria were used to draw boundaries of hypothalamic sub-regions. The criteria used to determine these boundaries are those used by Swanson (2004) and draw upon a wide variety of studies for each of the hypothalamic sub-regions depicted. Briefly, these include morphology, staining intensity, orientation, packing density and distribution as revealed in Nissl-stained sections (Simmons and Swanson 1993), an example of which is shown in **Figure 3, B**. The scope of the chemoarchitectural analysis performed includes atlas templates (atlas levels 23–30) covering two of the four major rostrocaudal divisions of the hypothalamus (anterior and tuberal). For each of these levels, the entire mediolateral and dorsoventral extents of the hypothalamus were analyzed. Based on their cytoarchitectural boundaries, tissue sections were identified as corresponding to one of the atlas levels observed in this study, which then allowed for the transfer of data from immunohistochemically-stained sections to atlas templates. Before this, however, boundaries that were established using an adjacent tissue series which was Nissl-stained are overlaid onto the immunohistochemically-stained sections with the use of separate data layers in the Adobe Illustrator platform (**Figure 3)**. This allowed for the approximate locations of all mapped cell bodies and fibers in this study to be determined and reported using atlas templates.

Three tissue series from different animals were each used in order to perform immunohistochemical stains for combinations of αMSH+H/O (n=3) and αMSH+MCH (n=3), respectively. The three cases that will be mapped for these αMSH+H/O combinations will allow

for comparison of the presence of these neuropeptides across different subjects. This will allow for statistical comparison to determine regions of lower and higher variability for presence of these neuropeptides and, eventually, of the locations for putative appositions between α-MSH-ir fibers and H/O-ir or MCH-ir somata, which will be discussed in further detail in the second aim of this project. The use of immunoperoxidase staining protocols to facilitate the analysis of putative appositions will also be discussed in the next section.

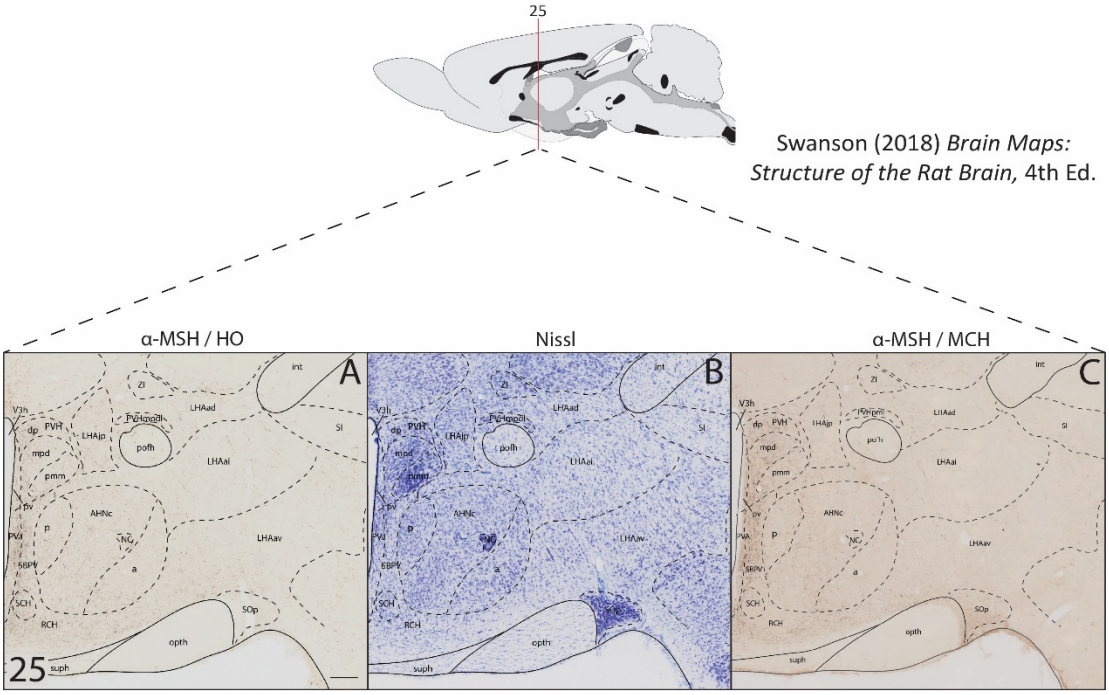

Figure 3. Examples of the quality of histology. **(A and C).** Representative sections stained for αMSH+HO or αMSH+MCH, respectively, which show overlaid parcellations from **(B).** A nissl-stained section. All three sections shown here represent three different adjacent tissue series from the same animal. Images were taken at ×10 magnification. Please consult the Appendix for an explanation of the abbreviations used in this figure. Scale bar in **Panel A** represents 200 µm and applies to all panels

---

III.1.1. Distribution of α-MSH-ir fibers throughout the hypothalamus

αMSH-ir fibers are more sparsely distributed in lateral structures; however, there is at least a small representation of these fibers in each hypothalamic sub-region throughout the rostrocaudal

extent of the analyzed levels. The highest concentration of fibers was observed in the medial and perifornical portions of the hypothalamus, with structures such as the PVa, PVi, PVHap, PVHpv, PVHmpd, PVHf, DMHa, DMHv and DMHp, having the most robust presence for αMSH-ir fibers. There are also some medial zone regions that seem to noticeably lack αMSH-ir fibers, such as the more caudally located VMHdm, VMHc, and more rostral parts of the AHN.

The distribution of αMSH-ir somata is strictly restricted to that of the ARH and immediately adjacent regions such as the TUsv, beginning from level 27 and continuing through the rest of the surveyed atlas levels. These distributions are consistent with previous reports (Guy et al 1982, Kiss et al 1984 and Jacobowitz et al 1978).

III.1.2. Distribution of H/O-ir fibers and somata throughout the hypothalamus

The density for H/O-ir fibers varies throughout the rostrocaudal extent of the hypothalamic atlas levels sampled in this study. More caudal levels have relatively equal distributions of fibers throughout the mediolateral extent of the hypothalamus, with the most rostral level sampled – atlas level 26 – demonstrating a higher density of fibers in the medial zone of the hypothalamus. Caudal levels also contain a greater number of fibers which remain within the image plane for longer distances and which have a higher presence in more dorsal regions (**Figure 4, E–H)**. This suggests that these fibers travel in a more lateral direction than the shorter fibers of more rostral sections, which are likely traveling in a rostrocaudal direction.

Consistent with previous studies, the highest density of cell bodies for H/O were observed within atlas levels 29 and 30, with the most anteriorly sampled cell bodies observed at level 27 for this specific case; however, previous studies have reported H/O-ir cell bodies as anterior as level

26 (Swanson et al 2005, Hahn 2010). These cell bodies form a band that spans several perifornical sub-regions, including the LHAjd, LHAs, LHAd and LHAma.

III.1.3. Possible synaptic interactions zones for αMSH-ir fibers and H/O-ir somata

By mapping the same neuropeptide combinations across three different animals, we are able to analyze patterns across subjects, in order to determine what regions might have areas of consistent peptide expression and, moreover, areas of consistent co-localization of immunoreactive fibers and cell bodies which have been dubbed as "possible synaptic interaction zones (PSIZ)" by previous studies in our laboratory (Wells 2017). In this study, three animals were used for testing a neuropeptide combination of H/O+αMSH immunostains, which will allow for the generation of maps demonstrating regions of high and low variability in peptide co-spatial occupancy in common sub-regions. Being able to identify these PSIZs with higher confidence will allow researchers who want to study the interactions of these neuropeptides to save time and effort and to narrow their search fields using more refined methods such as patch-clamp electrophysiology, optogenetics and electron microscopy; as they would be able to scan smaller regions in order to find neurons with the synaptic interactions they are seeking to study further.

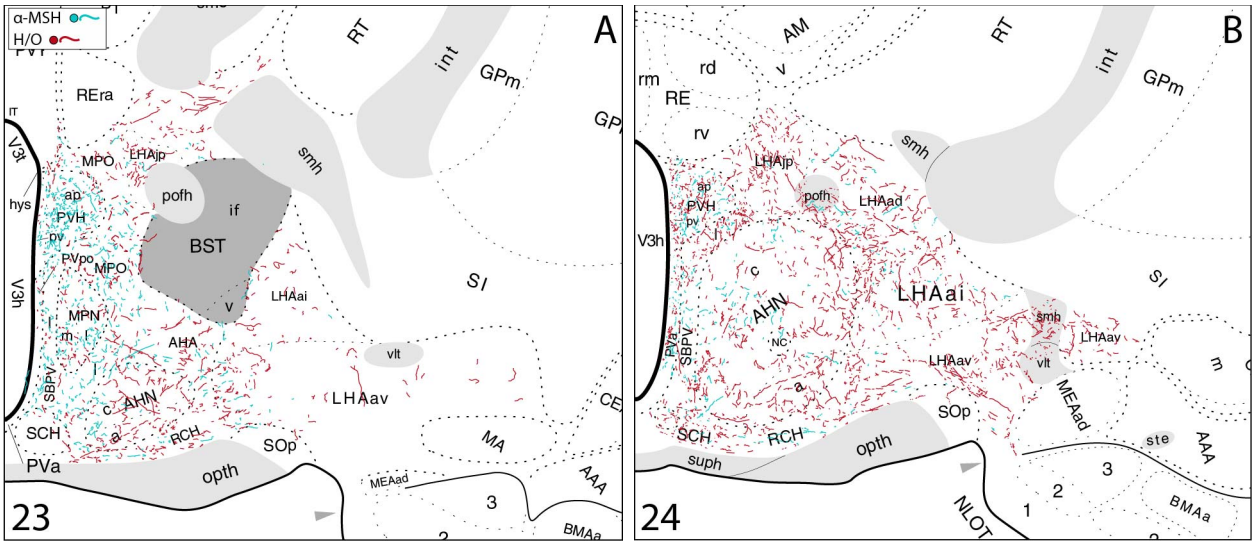

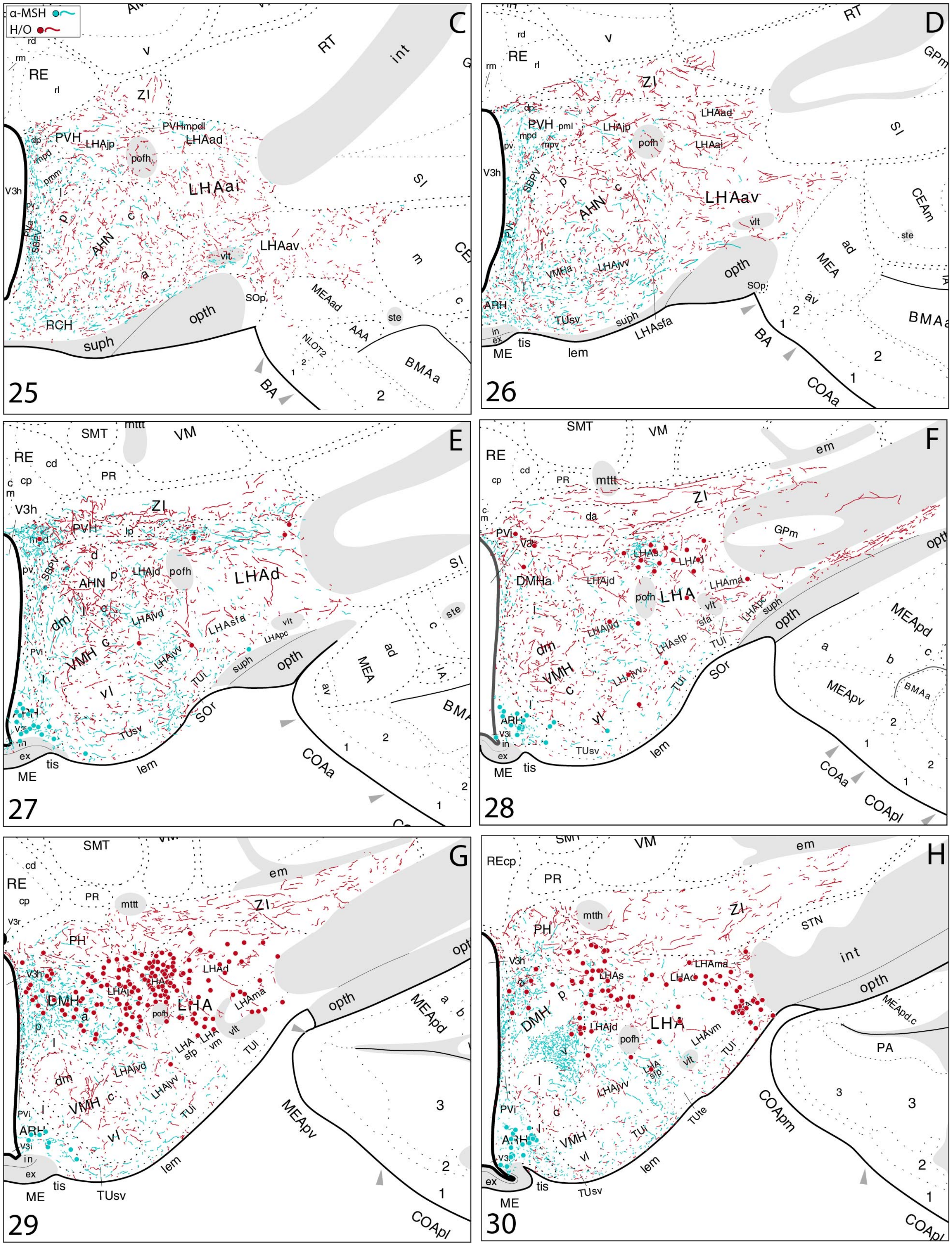
α-MSH
H/O
C
25
RE
ZI
PVH
PVHmpdl
LHAjp
LHAad
pofh
LHAai
AHN
LHAav
vlt
RCH
opth
suph
SOp
MEAad
AAA
ste
BMAa
BA
RT
int
SI
V3h
D
26
RE
ZI
PVH
LHAad
LHAjp
pofh
LHAai
AHN
LHAav
vlt
VMHa
LHAjvv
TUsv
ARH
ME
tis
lem
suph
LHAsfa
opth
SOp
BA
COAa
MEA
CEAm
BMAa
RT
GPm
SI
E
27
SMT
VM
RE
PR
ZI
PVH
AHN
LHAjd
pofh
LHAd
LHAjvd
LHAsfa
LHAjvv
LHApc
vlt
VMH
TUi
TUsv
SOr
opth
suph
ME
tis
lem
COAa
MEA
SI
F
28
SMT
VM
RE
PR
mtt
ZI
em
GPm
DMHa
LHAjd
LHAs
LHAj
LHAma
pofh
LHA
vlt
LHApc
LHAjvd
LHAsfp
LHAjvv
VMH
TUi
TUsv
SOr
opth
suph
ARH
ME
tis
lem
MEApd
MEApv
BMAa
COAa
COApl
G
29
SMT
RE
PR
mtt
ZI
em
PH
DMH
LHAd
LHA
LHAma
pofh
vlt
LHAjvd
LHAjvv
VMH
TUi
ARH
ME
tis
TUsv
lem
opth
MEApd
MEApv
COApl
H
30
SMT
VM
REcp
PR
mtth
ZI
em
STN
int
opth
PH
DMH
LHAs
LHAma
LHAd
LHAjd
LHA
pofh
LHAvm
vlt
LHAjvv
TUi
TUte
VMH
ARH
ME
tis
TUsv
lem
MEApd.c
PA
COApm
COApl

Figure 4. Representative maps for alpha-melanocyte stimulating hormone (αMSH) and hypocretin/orexin (H/O) chemoarchitecture from levels 23–30. Circles were used to denote neurons and lines for neuronal fibers. The BST sub-region is not part of the hypothalamus and was therefore not analyzed; in order to avoid the assumption that this region is devoid of neuropeptide signal it was grayed out. Blue was used to represent αMSH and red for H/O. Legends at the top left corner of **Panels A and G** represent the color-coding scheme for each neuropeptide shown. Data were translated onto the rat brain atlas templates from Swanson (*Brain Maps 4.0*; Swanson, 2018) and arranged from rostral to caudal: the atlas level is located at the bottom left corner of each panel. See Appendix I for a full list of abbreviations. N=1.

III.1.4. Distribution of MCH-ir fibers and somata throughout the hypothalamus

Fiber staining for MCH was not as robust as that observed for H/O-ir fibers; because of this, we are unable to comment in detail on the distribution of MCH-ir fibers. MCH-ir cell bodies are situated further dorsally than are H/O-ir cell bodies, with a large group of cells found within the ZI. The presence of MCH-ir cell bodies within the ZI persists throughout the rostrocaudal extent of sampled atlas levels containing this structure, beginning at level 26, where lower densities of MCH-ir cell bodies can be found (**Figure 5, D**) and which increase in density at more caudal levels. Contrary to previous reports (Hahn 2010, Swanson et al 2005), cell bodies were found to localize within the PVHmpd and PVHlp at level 27 within this single case. The presence of MCH-ir somata within the PVH may not be a common occurrence and could be a region of high variability for the presence of MCH; however, this study does not contain enough animals to explore that possibility. Consistent with previous reports, there is a band of MCH-ir cell bodies that extends across sub-regions surrounding the dorsal area of the *pofh* in regions such as the LHAjd, LHAs, LHAd, LHAma, LHApc and LHAvl. Other areas ventral to the fornix where groups of MCH cell bodies localize are the DMHa, DMHv, LHAjvv and LHAjvd. This is a similar pattern to that observed for the distribution of H/O-ir cell bodies. In contrast, MCH-ir cell bodies extend further laterally at atlas levels 28–30. MCH-ir cell bodies were not observed to localize to more

ventral sub-regions such as the VMH, ARH TUte, TUsv and TUi, for those levels where cell bodies were present in other areas.

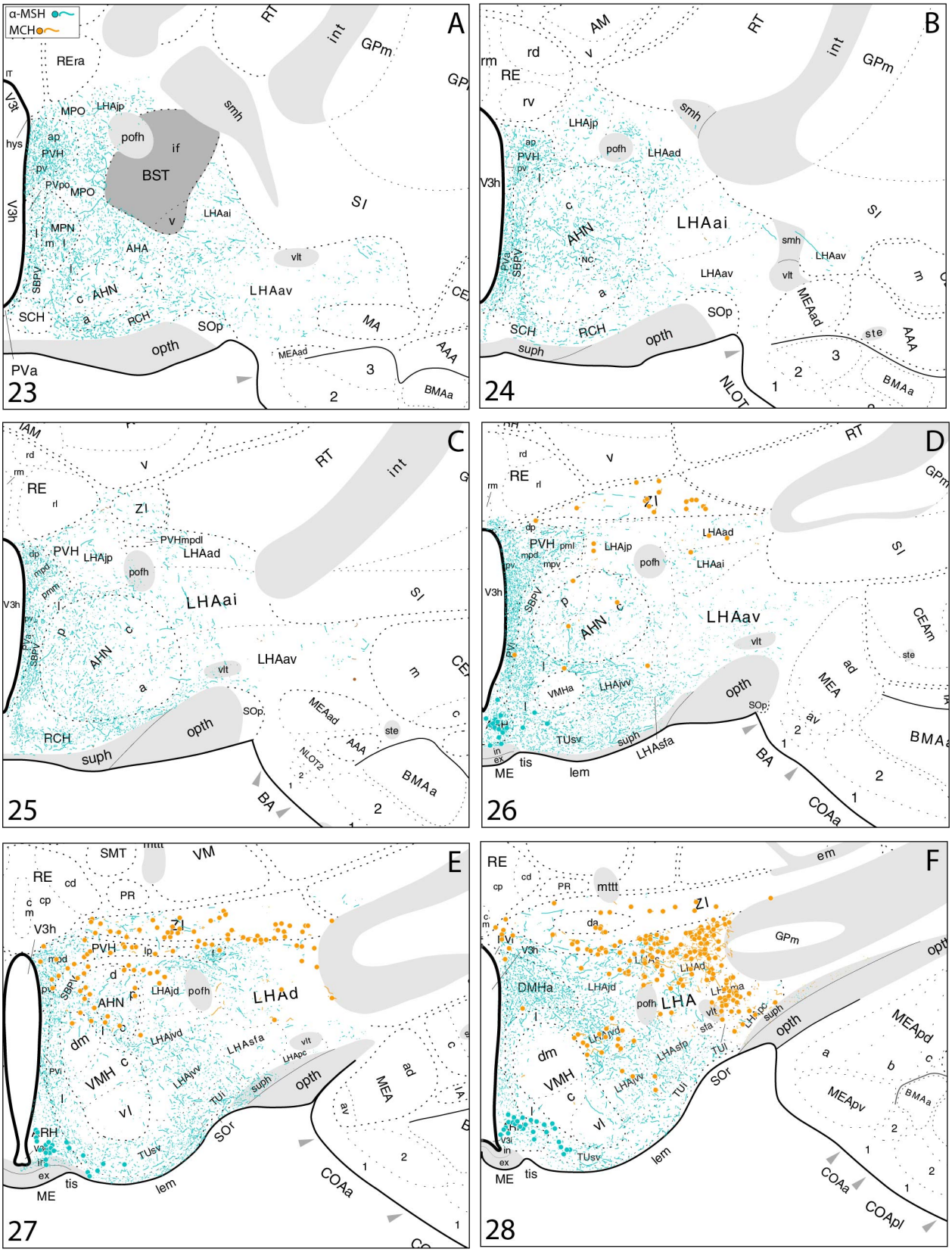

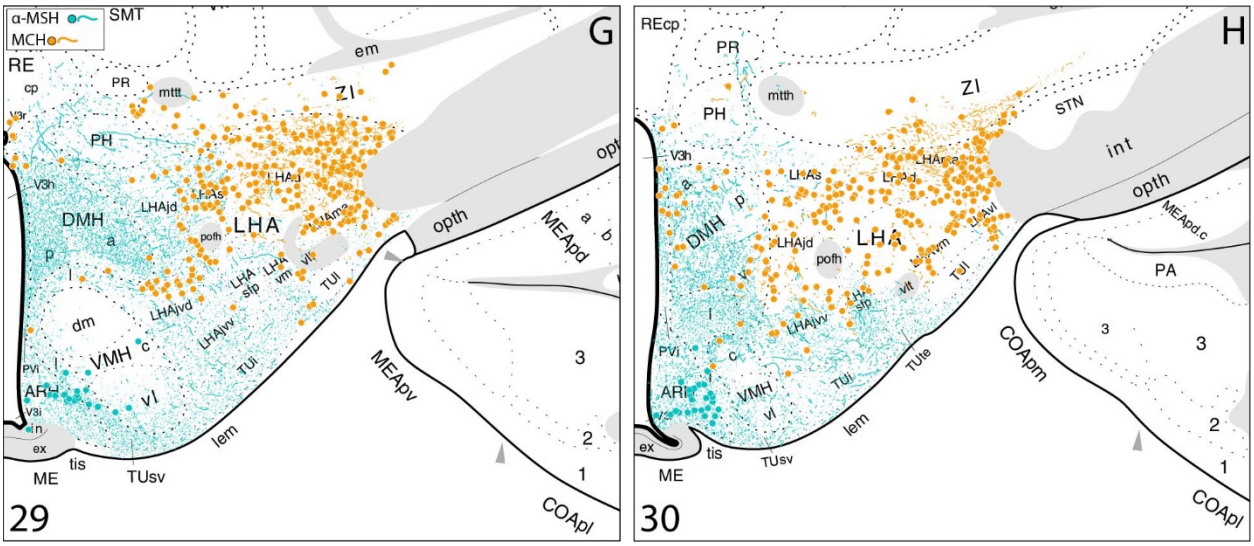

Figure 5. Maps for alpha-melanocyte stimulating hormone (αMSH) and melanin concentrating hormone (MCH) chemoarchitecture from levels 23–30. Circles were used to denote neurons and lines for neuronal fibers. Blue was used to represent αMSH-ir cell bodies and fibers. Orange was used for MCH-ir cell bodies and fibers. Legends at the top left corner of **Panels A and G** represent the color-coding scheme for each neuropeptide shown. Data were translated onto the rat brain atlas templates from Swanson (*Brain Maps 4.0*; Swanson, 2018) and arranged from rostral to caudal: the atlas level is located at the bottom left corner of each panel. See Appendix I for a full list of abbreviations. N=1.

III.2. Aim 2: To extend the predictive power of atlas-based mapping by identifying and mapping the distributions of putative αMSH-ir axonal appositions with H/O- or MCH-ir cell populations using the Swanson reference atlas.

Using the Adobe Illustrator files containing the annotated images of the immunoperoxidase-labeled material as a reference, stained tissue sections were analyzed under ×100 magnification in order to determine which of the cells contained putative appositions according to the criteria outlined in the Methods. By using the annotated images, we can ensure that the cells we observed to contain putative appositions could be overlaid onto the cytoarchitectural boundaries determined by our analysis of Nissl-stained sections, as was performed for Aim 1. This procedure allows us to demonstrate the spatial distributions of these putative appositions using the same spatial framework to qualitatively depict these distributions

(**Figures 7 and 9).** Most putative interactions observed contained one or two boutons; however, some were observed to involve more than two boutons that were seemingly in contact with the analyzed soma.

III.2.1. αMSH-ir fibers– H/O-ir somata: Distributions of putative appositions

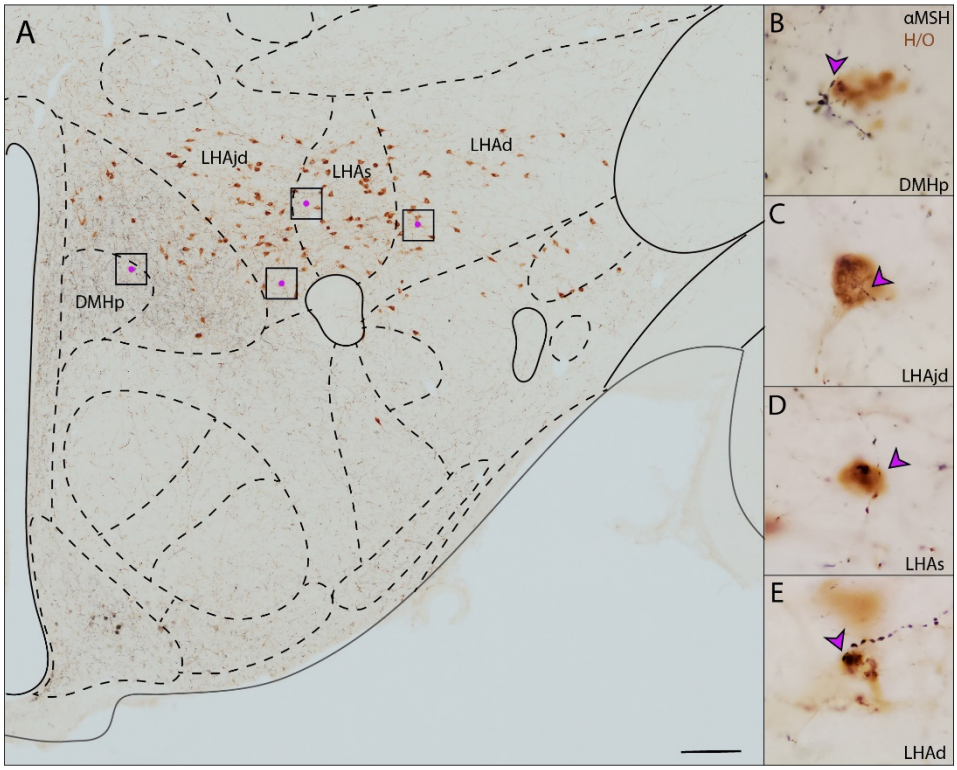

Figure 6. Examples of putative appositions of α-MSH-ir fibers with H/O-ir somata. **(A).** Stitched image, at ×10 magnification, of a DAB-stained section with purple dots depicting the location of H/O neurons with positive putative appositions through the hypothalamus. **(B–E).** Images at ×100 magnification taken with a Samsung Galaxy S10+ through an Olympus BX53 microscope showing α-MSH-ir fibers in the same focal plane as H/O-ir somata. These are the visual criteria taken into consideration when surveying tissues to identify putative appositions. Scale bar in **Panel A** represents 200 µm.

Spatial distributions of H/O-ir somata containing putative appositions from αMSH-ir fibers mostly correlated with areas where co-expression of H/O and αMSH was in high density. The majority of putative appositions were mostly located medially and did not extend to lateral regions (**Figure 7, level 29** shows an illustrative example of this). DMHa, LHAjd, and LHAs were some of the areas showing the highest density of putative appositions. The LHAs was one of the areas containing a

high density of H/O-ir cell bodies through **levels 27–30,** but only a small portion of those cells showed any putative interactions with α-MSH-ir fibers. In fact, level 28 had no putative appositions in the LHAs, even though there were a number of H/O-ir cell bodies present. **Figure 5 F and G** illustrates a uniform distribution of H/O-ir cell bodies and αMSH-ir fibers, eliminating the possibility that the absence of interactions was due to the fibers or cell bodies not being properly stained. Other example areas where the same labeling can be observed were the LHAd and LHAvl at **level 30**.

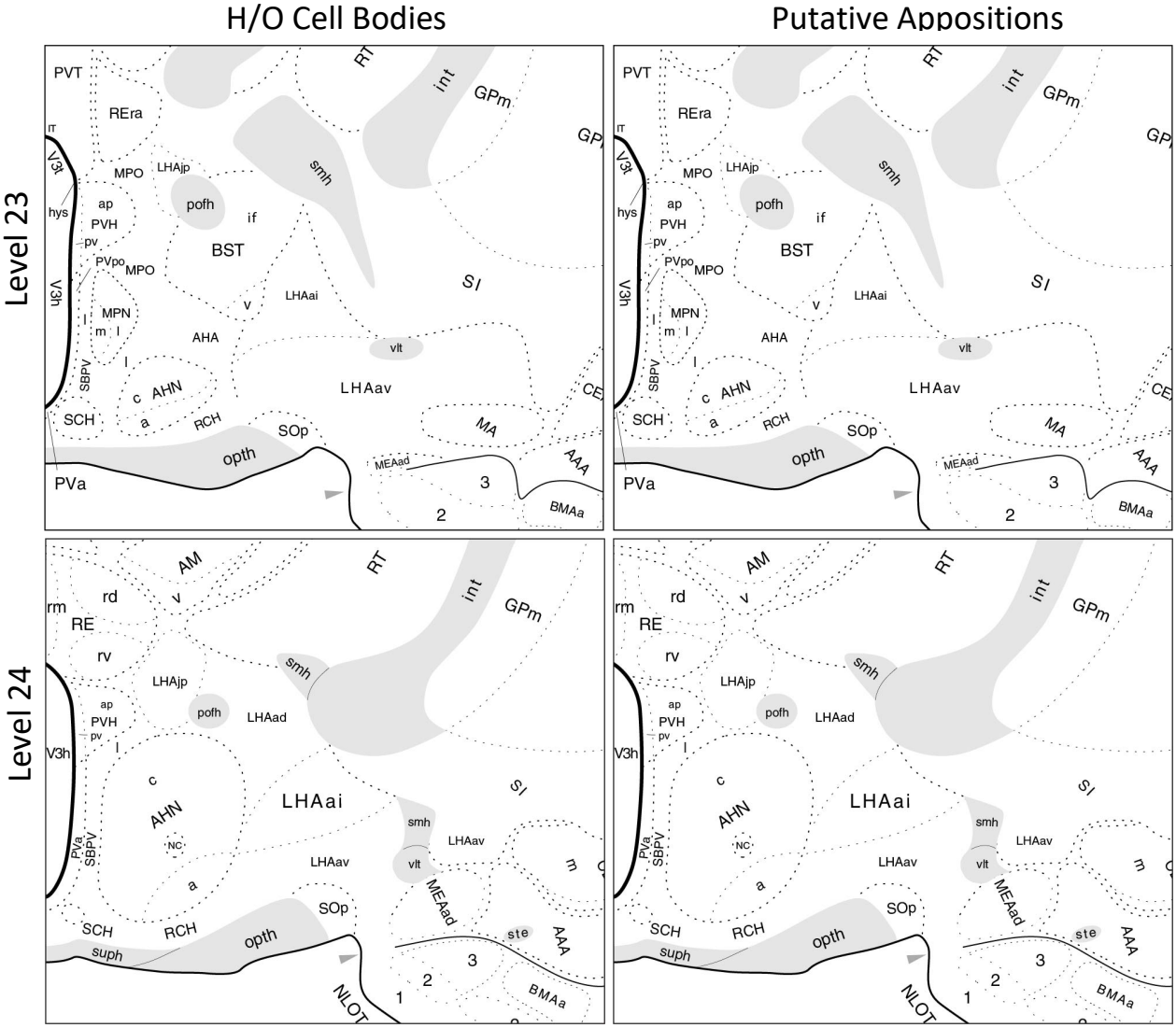

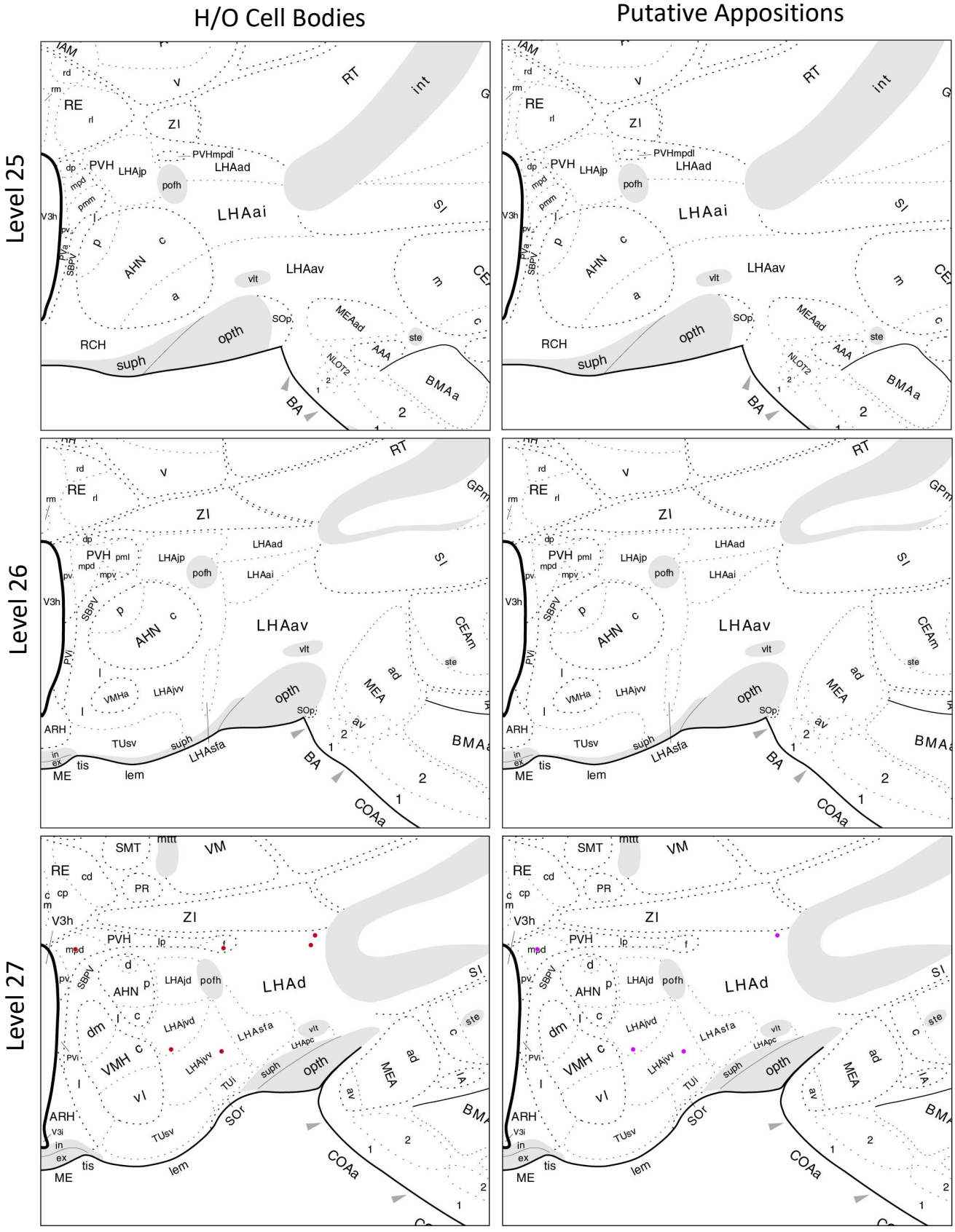
H/O Cell Bodies
Putative Appositions
Level 25
Level 26
Level 27
IAM
rd
rm
RE
rl
v
ZI
RT
int
PVH
dp
mpd
pmm
PVHmpdl
LHAjp
LHAad
pofh
LHAai
V3h
pv
SBPV
PVa
p
l
AHN
c
a
LHAav
vlt
SI
m
CE
RCH
opth
SOp
MEAad
ste
AAA
suph
NLOT2
BMAa
BA
pml
mpv
GPm
VMHa
LHAjvv
ad
MEA
CEAm
ARH
TUsv
LHAsfa
av
ME
in
ex
tis
lem
COAa
SMT
mttt
VM
cd
cp
PR
dm
VMH
vl
LHAd
LHAjd
LHAjvd
LHAsfa
vlt
LHApc
TUi
SOr
IA
V3i

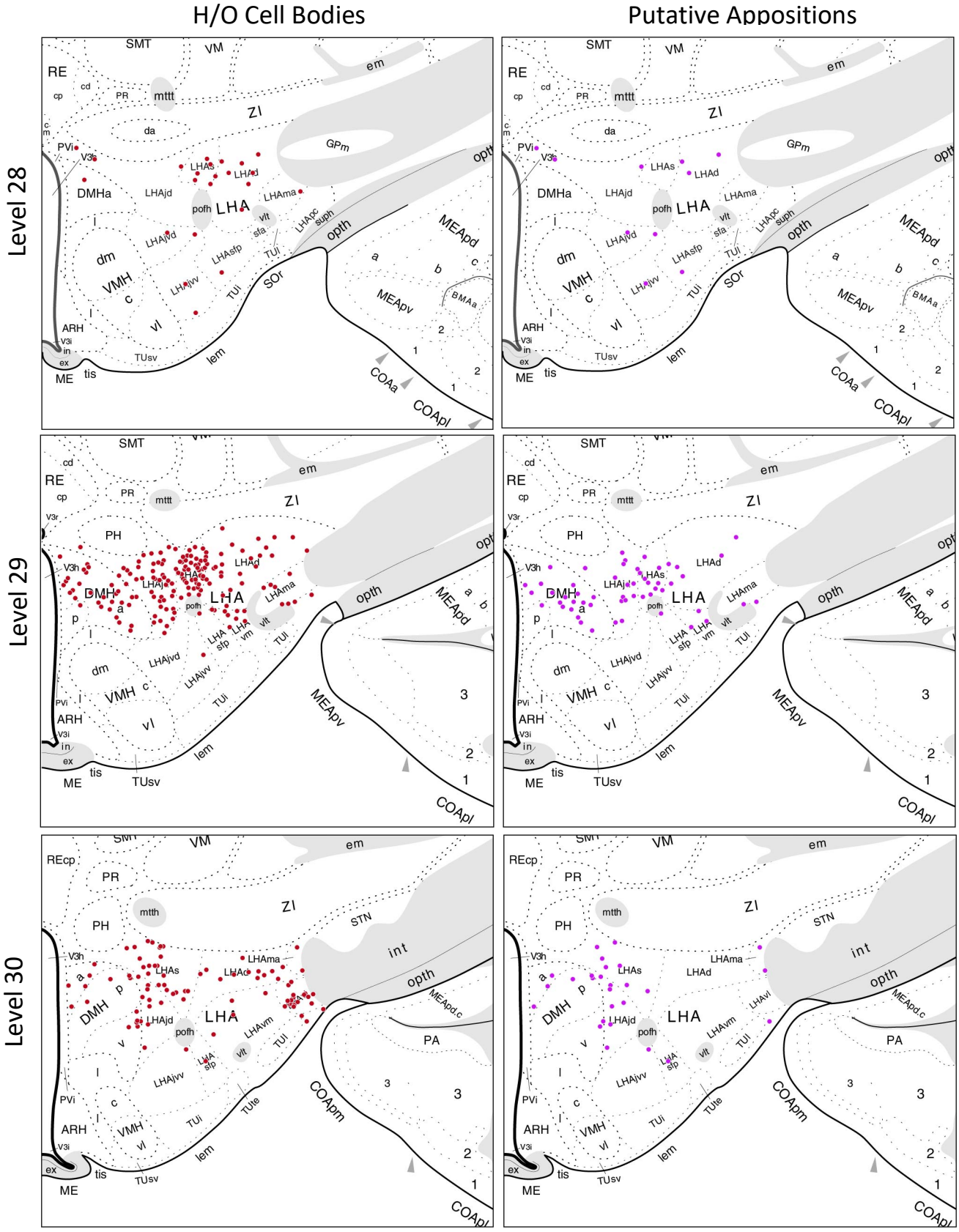
H/O Cell Bodies
Putative Appositions
Level 28
Level 29
Level 30
SMT
VM
em
RE
cp
cd
PR
mttt
ZI
da
GPm
PVi
V3h
LHAs
LHAd
DMHa
LHAjd
pofh
LHA
LHAma
vlt
sfa
LHApc
suph
opth
MEApd
dm
VMH
LHAjvd
LHAsfp
TUl
SOr
a
b
c
l
vl
LHAjvv
MEApv
BMAa
ARH
V3i
in
ex
TUsv
lem
ME
tis
COAa
COApl
1
2
3
PH
V3r
DMH
p
v
LHAvl
LHAvm
LHA sfp
LHA vm
PVi
RECp
mtth
STN
int
PA
MEApd,c
COApm
TUte

Figure 7. Representative maps for hypocretin/orexin (H/O) cell body distribution (*left column*) and distribution of the subset of those cells receiving possible synaptic input from αMSH-ir fibers (*right column*). Distributions from levels 23–30 are shown in a rostral to caudal atlas level organization, from top to bottom. Circles were used to denote neurons in both sets of maps. Red is used for H/O and pink is used for those H/O-ir cells that were considered to contain putative appositions from αMSH-ir fibers when analyzed under the oculars at ×100 magnification. Data were translated onto the rat brain atlas templates from Swanson (*Brain Maps 4.0*; Swanson, 2018). See Appendix I for a full list of abbreviation. N=1.

III.2.2. αMSH-ir fibers –MCH-ir somata: distributions of putative appositions

Unlike H/O, the presence of MCH-ir putative appositions did not correlate with the presence of the neuropeptide at all levels. A smaller number of MCH-ir cell bodies were found to have putative appositions when compared to H/O-ir cell bodies. MCH-ir somata were observed in the ZI, LHAad, LHAjp, and AHNc **(Figure 9, Level 26)**. Yet none of these were found to be positive for putative appositions. This trend was observed throughout the most rostral levels containing MCH-ir somata (**atlas levels 26 and**

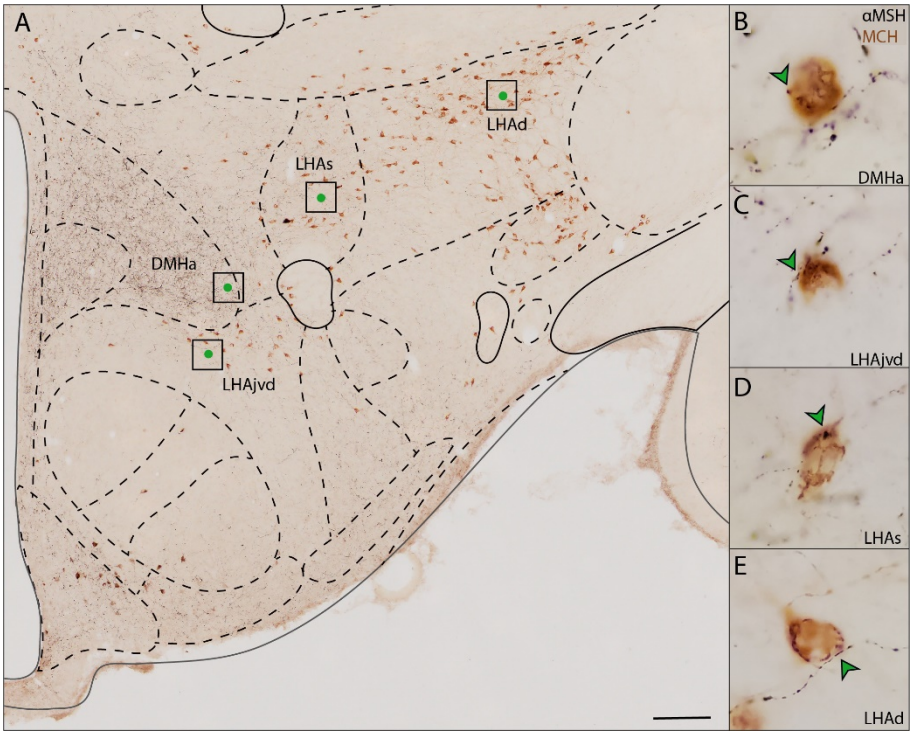

Figure 8. Examples of putative appositions of α-MSH-ir fibers and MCH-ir somata. **(A).** Stitched image, at ×10 magnification, of a DAB-stained section with green dots depicting the location of MCH neurons with positive putative appositions through the hypothalamus. **(B–E).** Images at ×100 magnification taken with a Samsung Galaxy S10+ through an Olympus BX53 microscope showing α-MSH-ir fibers in the same focal plane as MCH-ir somata. Scale bar in **Panel A** represents 200 µm.

27). However, **levels 28 and 29** shown a more lateralized distribution of putative appositions along perifornical regions. The one level that breaks this pattern by having a more periventricular distribution is **level 30,** although there is a small number of putative appositions located more laterally. Regions with a consistently large number of putative appositions at more than one atlas level include the LHAs, LHAd, LHAma, and LHAjvd. One region worth highlighting is the LHAd, which displayed the largest number of MCH-ir somata, but did not contain many putative appositions. Many of these differences could be caused by the lack of αMSH-ir fibers located in the more lateral zone sub-regions of caudal levels, with higher densities found in more periventricular zone nuclei.

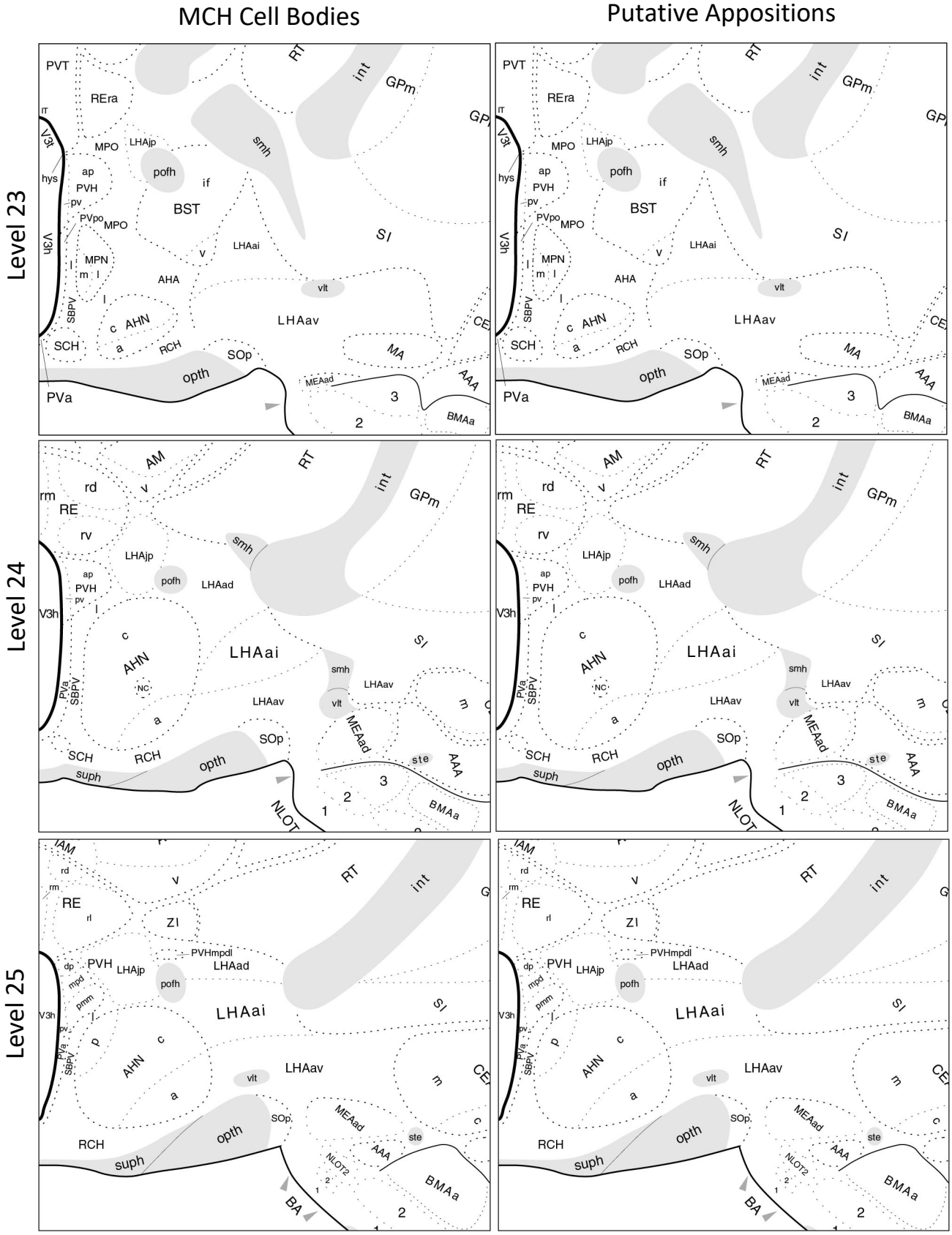
MCH Cell Bodies
Putative Appositions
Level 23
Level 24
Level 25
PVT
RT
int
GPm
REra
MPO
LHAjp
smh
pofh
if
BST
SI
PVH
PVpo
LHAai
MPN
AHA
vlt
LHAav
AHN
SCH
RCH
SOp
MA
CE
opth
MEAad
AAA
PVa
BMAa
AM
rm
rd
v
RE
rv
ap
pv
l
V3h
c
a
SBPV
NC
ste
m
suph
NLOT
RL
ZI
PVHmpdl
LHAad
dp
mpd
pmm
p
BA

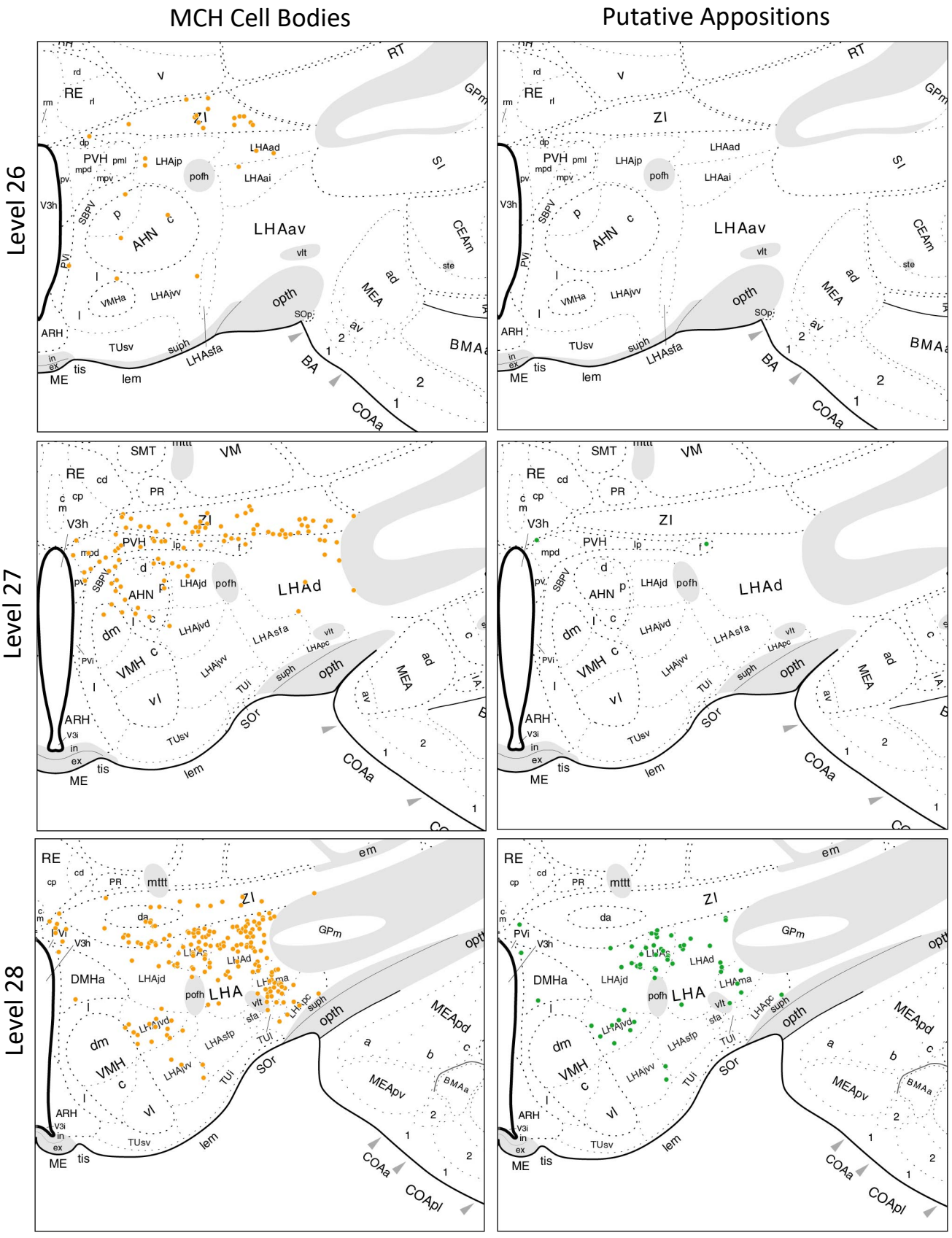
MCH Cell Bodies
Putative Appositions
Level 26
Level 27
Level 28
RE
ZI
RT
GPm
SI
PVH
LHAjp
LHAad
LHAai
pofh
LHAav
CEAm
AHN
VMHa
LHAjvv
opth
MEA
ad
av
BMAa
ARH
TUsv
suph
LHAsfa
BA
ME
tis
lem
COAa
SMT
VM
PR
LHAjd
LHAd
dm
VMH
LHAjvd
LHAsfp
TUl
SOr
vlt
LHApc
vl
DMHa
LHA
LHAma
MEApd
MEApv
COApl

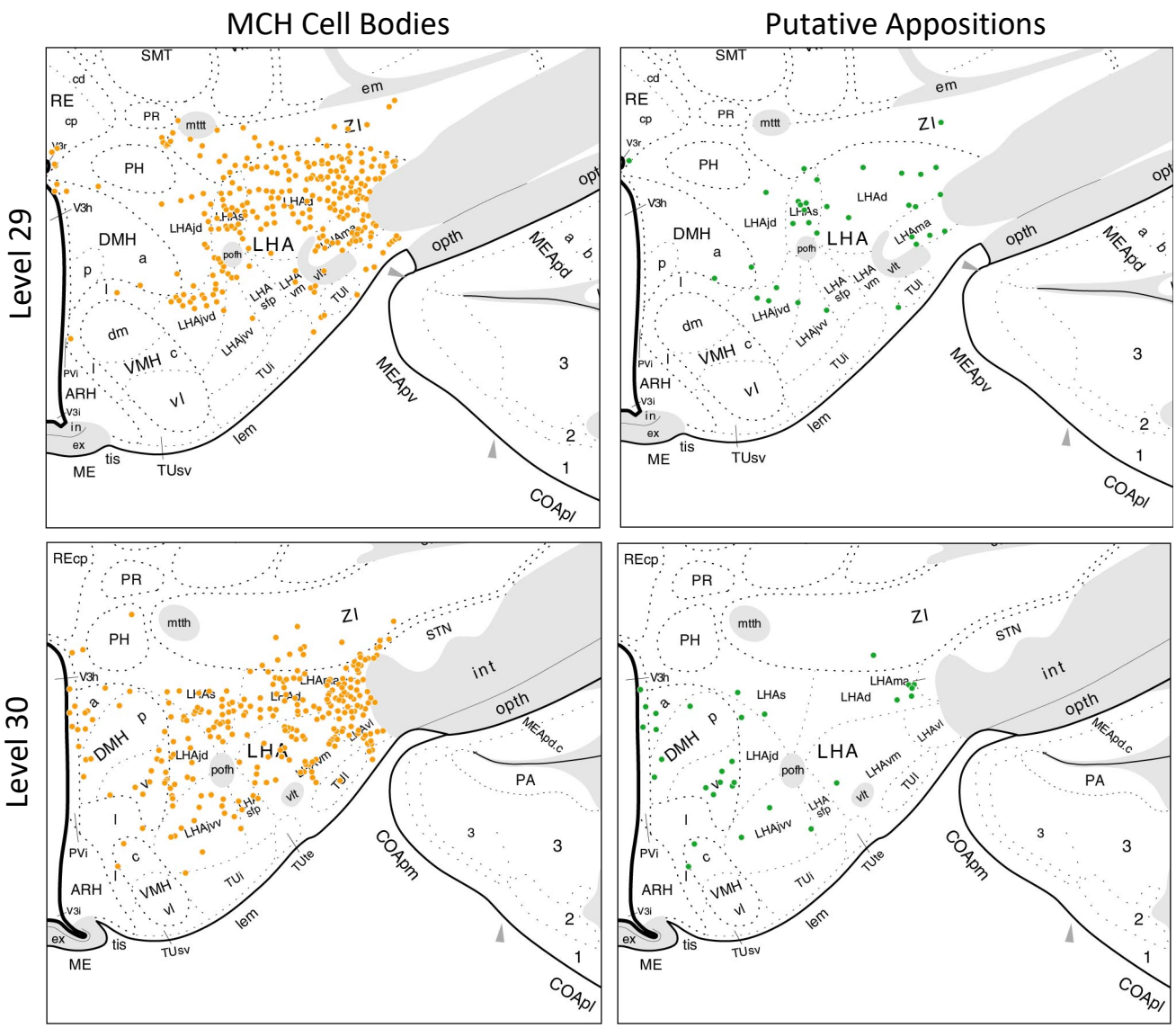

Figure 9. Maps for melanin-concentrating hormone (MCH) cell body distribution (*left column*) and distribution of the subset of those cells receiving possible synaptic input from αMSH-ir fibers (*right column*). Distributions from levels 23–30 are shown in a rostral to caudal atlas level organization, from top to bottom. Circles were used to denote neurons in both sets of maps. Orange was used for MCH and green was used for those MCH-ir cells that were considered to contain putative appositions from α-MSH-ir fibers when analyzed under the oculars at ×100 magnification. Data were translated onto the rat brain atlas templates from Swanson (*Brain Maps 4.0*; Swanson, 2018). See Appendix I for a full list of abbreviations. N=1.

III.2.3. Semi-quantitative analysis of putative appositions

Semi-quantitative cell counts were manually performed for each of the hypothalamic sub-regions throughout the extent of the levels analyzed. These cell counts were performed using the atlas maps presented in **Figure 9**. These atlas maps contain each of the hand-annotated cell bodies for both chemoarchitecture as well as putative appositions from immunoperoxidase-stained material. Annotated cell bodies were placed by examining their photomicrographs, and these cell body annotations were later refined as putative apposition analysis was carried out under ×100 magnification in order to increase the accuracy of cell counts, with special care taken to ensure that each cell was placed in their respective hypothalamic sub-regions. The data obtained from these counts provide information about the relative proportions of cells located in each hypothalamic sub-region and the amounts of those cells which contain putative appositions. In combination with the spatial distributions of putative appositions, the semi-quantitative data given here allow for enhanced analysis of the data presented.

III.2.3.1 Single representative case analysis

When observing the percentages of distributions for putative appositions by level, it was found that H/O received the highest percentage of putative appositions with αMSH-ir elements in level 29 (52%), which is consistent with the percent of total H/O-ir neurons found in level 29 (58%: **Figure 10 B**). This, however, only represents 34% of the total number of H/O-ir neurons found in level 29. Of these neurons containing putative appositions in level 29, the regions found to contain the most putative appositions were the DMHa (33%), LHAjd (25%) and LHAs (18%). Across all levels, it was observed that the three hypothalamic sub-regions containing the most appositions of αMSH-ir fibers onto H/O-ir cells were the LHAjd, DMHa and LHAs.

Interestingly, putative appositions of αMSH-ir fibers with MCH-ir cells, had the highest percentage at level 28 (46%), which does not contain the highest percentage of total MCH-ir cells (22%), as compared to level 30 (32%: **Figure 10 D**). The number of putative appositions in level 28 accounts for 29% of the total number of MCH-ir neurons at level 28. The regions with the highest percentage of putative appositions for level 28 are the LHAs (37%) and LHAd (22%). The fact that the LHAs at level 28 has the highest number of raw putative appositions of any single sub-region at any single level, accounting for 65% of the total number of MCH-ir cells in this sub-region, is also of note. Overall, across all levels, the regions with the greatest number of αMSH–MCH putative appositions were the LHAs, LHAd and LHAjvd.

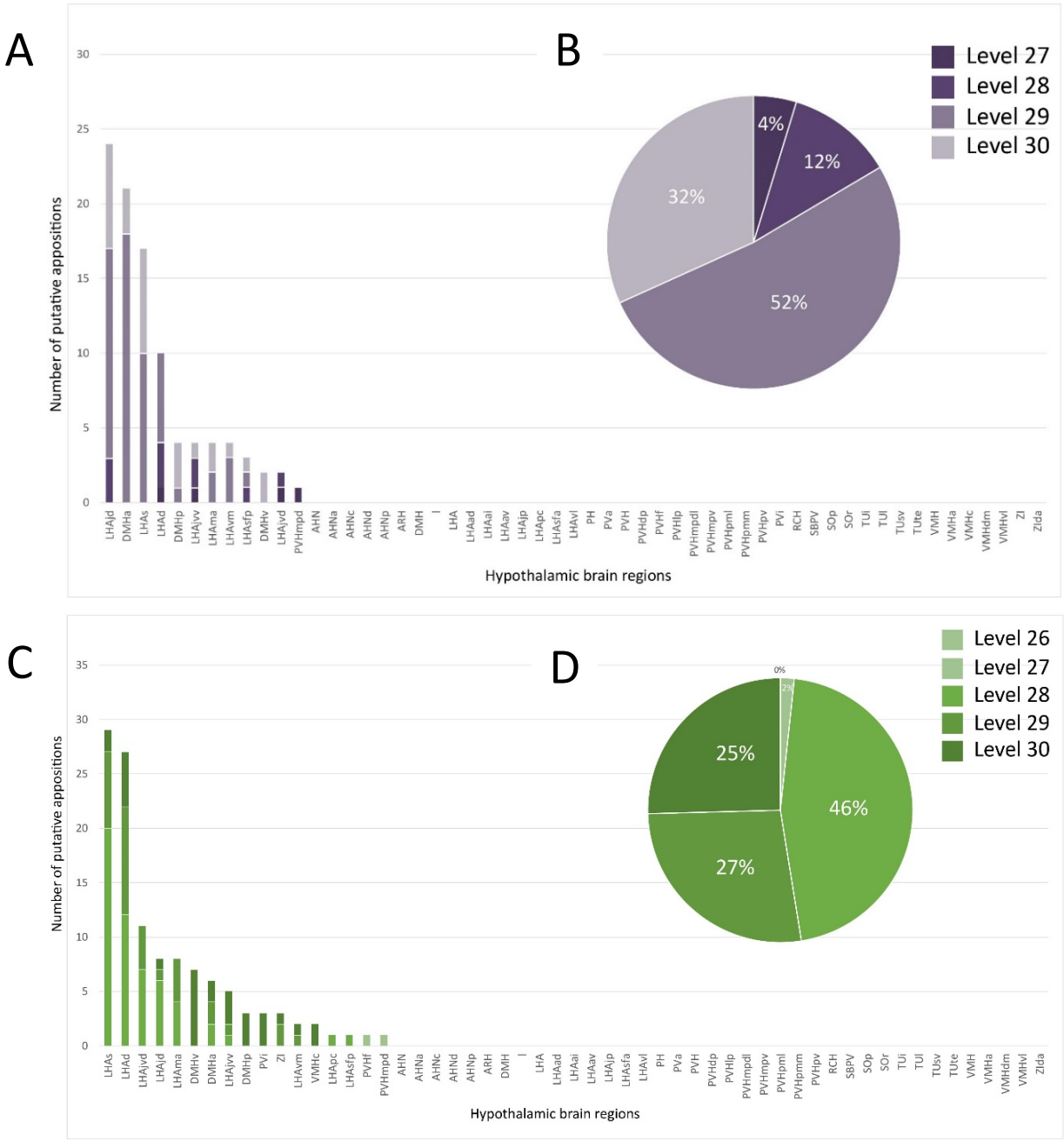

Figure 10. Quantification for putative appositions from αMSH-ir fibers onto H/O- or MCH-ir somata. **Panels A and C** show bar graphs of the total counts for H/O- and MCH-ir somata, respectively, containing putative appositions from αMSH-ir fibers. The counts are subdivided by color in order to demonstrate how many cells from each sub-region were found at each atlas level analyzed. N=1. **Panels B and D** demonstrate pie charts for the percentages of total putative appositions found at each atlas level analyzed. N=1. Please consult the Appendix for a list of terms corresponding to the abbreviations in these graphs.

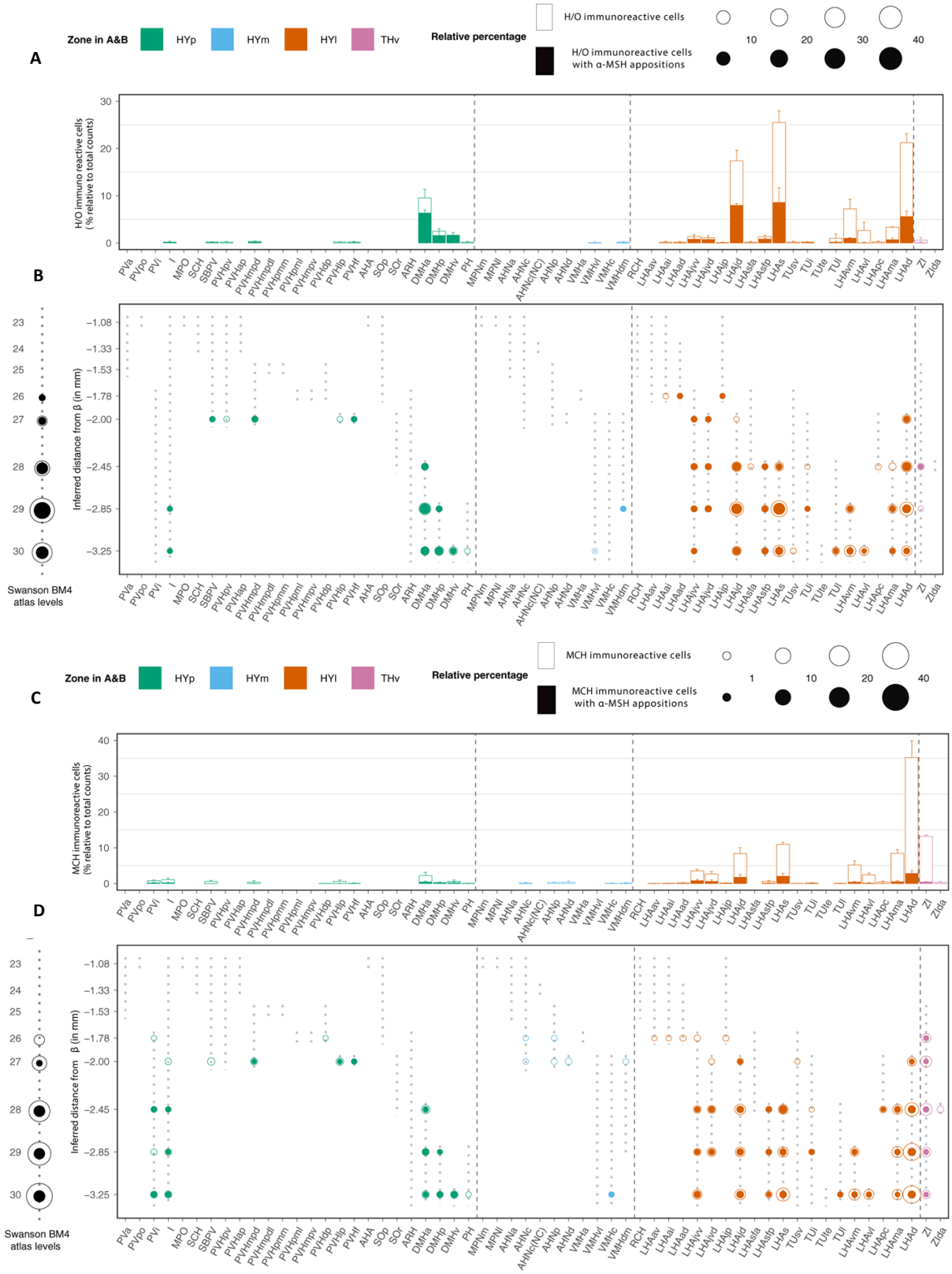
A
Zone in A&B
HYp
HYm
HYl
THv
Relative percentage
H/O immunoreactive cells
H/O immunoreactive cells with α-MSH appositions
10
20
30
40
H/O immuno reactive cells (% relative to total counts)
B
Inferred distance from β (in mm)
Swanson BM4 atlas levels
C
MCH immunoreactive cells
MCH immunoreactive cells with α-MSH appositions
1
10
20
40
MCH immunoreactive cells (% relative to total counts)
D
Inferred distance from β (in mm)
Swanson BM4 atlas levels

Figure 11. Bar graph and dot plot representations of relative percentages for H/O- (**A and B**) and MCH-ir (**C and D**) somata found to contain putative contacts from αMSH-ir fibers. Please consult Appendix I for a full list of terms corresponding to the anatomical abbreviations shown on these charts. Charts provided courtesy of Dr. Sivasai Balivada of the Khan laboratory.

III.2.3.2 Analysis across multiple cases

The trends observed in the counts from the representative case used to generate the graph of H/O-somata containing putative appositions from αMSH-ir axonal fibers in **Figure 10 (A and B)** hold when comparing them to the results for cell counts across regions of three cases. Observing the average percentages, by level, for H/O-ir somata with putative appositions from αMSH-ir fibers, we found that the percentages change with a range from 2–10%; yet, relative distributions of these remained constant with those reported in **Figure 10** (**B**). When comparing sub-regions containing the largest average counts for these same putative appositions, we observed that the average counts are also very similar to that of the representative case. Most importantly, we observed that the top five areas remain constant, but changed in order: LHAs (30 ± 6.1 somata), LHAjd (28 ± 1.9 somata), DMHa (22 ± 1.39 somata), LHAd (21 ± 3.1 somata), and DMHp (5.3 ± 1.7 somata). Overall, this consistency between the representative case and averages across cases allows us to state with some degree of confidence that these regions will likely remain consistent when examining putative appositions from αMSH-ir fibers onto H/O-ir somata across different animals. In contrast, when observing the number of MCH-ir somata with putatively apposing αMSH-ir fibers in the representative case (**Figure 10C, D**), we observed that the trends of levels with the highest average putative appositions shifts to an almost equal distribution from levels 28–30, with 33%, 30% and 35% respectively, of average counts when compared across cases. Similar to what we observed with αMSH–H/O putative appositions, the top three regions in **Figure 10** (**C**) are the same top three regions when we take the average of MCH-ir somata with appositions across

all three cases; although we also observe that their order based on counts is rearranged. Specifically, when observing the average number of putative appositions between MCH-ir somata and αMSH-ir fibers across hypothalamic subregions, the LHAd (22 ± 4.72 somata) contains the highest average with the LHAs (18 ± 3.7 somata) containing the second-highest average number of putative appositions, and finally, the LHAjd (16.33 ± 3.7 somata) with the third-highest average number of putative appositions.

III.2.3.3 Analysis of relative percentages

As we shift our analysis from observations of the total number of somata with appositions from αMSH-ir fibers to the relative percentages of these, we have confirmation of the general trends observed in the counts, while at the same time being offered a new perspective on how we interpret these data. Taking a quick survey of **Figure 11,** we are quickly able to observe that the same areas that contain the highest numbers of putative appositions have the highest percentages of these which is expected. However, in this same figure, we are also clearly able to see that H/O-ir somata had a much higher relative percentage of appositions with αMSH-ir fibers when compared to MCH-ir somata. This can be observed both across regions and across levels. Similarly, we gain new insight when looking at the relative percentages of H/O-ir somata with apposing αMSH-ir fibers. Here, we observe that even though the LHAd, LHAs and LHAjd contain the highest percentages of total appositions, these coincide with the highest percentages of H/O-ir somata across cases. However, the DMHa, DMHp and DMHv become a lot more interesting when taking into account that even though they contain a lower percent total of H/O-ir somata, a much higher percentage of these have apposing αMSH-ir fibers. This implies that those H/O-ir somata within the subregions of the DMH are seemingly more directly targeted by αMSH-ir fibers. A similar trend can be observed when analyzing the relative distribution of appositions across levels,

where even though levels 26 and 27 contain lower percentages of appositions, these account for a higher percentage of the total H/O-ir somata within those levels. Similar results are apparent when we analyze the relative percentages of MCH-ir somata with apposing αMSH-ir fibers. Even though the LHAd, LHAs, and LHAjd contain the highest percentages of these putative appositions ,we can appreciate that these account for a very low percentage of total MCH-ir somata located within these regions. Interestingly, when we observed the DMH, even though there are very few MCH-ir somata within these subregions, most of these had apposing αMSH-ir fibers. Interpretation of these results, however, is difficult, as it could be that these have a stronger physiological role because there are so few of them or it could be that they happen so infrequently that there is no major functional effect from these. The most obvious take-away from these data is the obvious difference in the targeting of H/O-ir somata from αMSH-ir fibers when compared to MCH-ir somata. It would appear that there is a stronger relationship between αMSH-ir fibers and H/O-ir somata which may or may not have some physiological significance.

Chapter IV: Discussion

IV.1. Trends

The mapping of αMSH has been performed previously (Jacobowitz and O'Donohue et al 1978). However, these maps were not created in relation to any standardized atlas, which means that direct comparisons between our data and those data are not able to be performed in a straightforward way. This point aside, the hypothalamic regions where they found αMSH-ir fibers are in general agreement with those being reported in the current study. As far as the presence of αMSH-ir somata is concerned, it was also found to localize to the ARH and immediately adjacent areas. Overall, the study presented here provides a general confirmation of the study performed by J. D. Hahn (2010), and extends it by providing detailed distributions of the fiber systems in addition

to the cell body distributions for the neuropeptides examined. In his study, Hahn mapped H/O- and MCH-ir somata distributions across hypothalamic levels 25–33 of the Swanson rat brain atlas. In that study, the goal was to show possible differences between various subsets of neurons in the LHA-expressing H/O or MCH neuropeptides. One major difference between the maps shown here and those in Hahn 2010 is a difference in the number of animals represented on the maps furnished. Hahn 2010 represents five animals together on one set of maps, while in the current study we have one representative case per map, which makes a direct level-by-level visual comparison in quantitation difficult. Taking this point into consideration, we are still able to make comparisons in the trends observed. Here, we decided to represent only one case in order to be able to observe the numbers and trends of these cell somata with less visual clutter and to provide the reader a realistic expectation of what s/he would observe when performing IHC in a single animal. When examining similarities between our study and that of Hahn 2010, we find that levels 28 and 29 are the levels which contain the highest number of H/O- and MCH-ir somata. However, when examining level 28, it is worth mentioning that the LHAjd had the highest concentration of H/O-ir somata clustered closely to the *pofh* in Hahn 2010, while in the present there are only two neurons in the immediate area of the *pofh*. Similarly, when examining level 30, we can observe that the LHAvl in Hahn 2010 paper contains no H/O-ir somata, while here we see that this sub-region is one with a significant representation of H/O-ir somata at level 30.

Turning our attention to MCH, we are able to observe that the most rostral presence of MCH is located within level 25 in the ZI of Hahn 2010 with only one soma present, while here we did not find any MCH-ir somata before level 26. The ZI has a consistent presence of MCH-ir somata across levels 26–30; however, a subtle but noticeable difference is observable at level 26, with MCH-ir neurons concentrating in the more lateral ZI in the present study while the presence of

these is found in the more medial ZI in Hahn 2010. Another more notable discrepancy between the current study and that of Hahn 2010 is the presence of MCH-ir somata in the PVH. Hahn makes specific mention of the absence of MCH-ir somata within any subdivision of the PVH, which is also consistent with the observations made in the published work of Saper et al 1986 and Broberger et al 1998. In our study, we are able to observe a sizeable representation of MCH-ir somata throughout the PVH at level 27, specially within the PVHmpd and PVHlp, which show the same number of somata. There are a few possible sources for the variability between these two sets of studies. There always exists the possibility that there was a difference in the way that the two studies performed their mapping, with the most likely area of variation being the parcellation step. This, however, seems unlikely, as both sets of studies were conducted using the same criteria for defining what constitutes a cytoarchitectural boundary with respect to the PVH. Another possible source of variability is that there was a difference in the neuropeptide that was being immunocytochemically stained. This could be of consideration because MCH is derived from the same precursor pre-melanin concentrating hormone (PMCH) as other hypothalamic peptides NEI and NGE. If there was a discrepancy in the cross-reactivity of our MCH antibody, there is a chance that we are also looking at the presence of NEI or NGE, with the most likely of these being NEI. Previous studies demonstrated that both NEI and MCH have been observed to co-express within the same regions of the hypothalamus including the LHA and ZI (Bittencourt et al 2008). The fact that both neuropeptides co-localize gives us reason to believe that this will not be a concern. However, in order to confirm that we are only detecting the presence of MCH-ir somata, we have recently received the same antibody that was used by Bittencourt et al 1992 and which has been confirmed to have exclusive specificity to MCH. This will be a future direction that will be carried

out in order to strengthen the present study and will also be included when these data are submitted for publication.

Other similarities in trends across studies can be observed in the immediate regions surrounding the AHN at level 27, where it would seem that MCH has minimal representation within the AHN and yet there is a large number of MHC-ir somata directly surrounding these sub-regions. Even more consistency across studies can be seen at level 28, which shows the highest number of MCH-ir somata in both studies. This consistency even carries into the regional localization of the MCH-ir somata, where they were observed within the LHAs, LHAjd, and LHAma. If we assess similarities by level, we observe that out of the levels which overlap in both studies, MCH-ir somata have the most consistent presence at levels 29 and 30. Level 29 MCH-ir somata are located mostly in the lateral zone, with the LHAs, LHAd, LHAma, and LHAjvd containing most of these, with a comparatively lower presence in the LHAjd. In the same way, level 30 of both studies shows a preference for perifornical regions, with the highest presence of MCH-ir somata being found in the more lateral LHAd and LHAma sub-regions.

While Hahn 2010 represents multiple animals in one set of maps, the relative visual densities and trends can be compared and show a high degree of consensus with few regions of major discrepancies with the current study. A comparison of this nature is possible because the datasets were mapped to the same standardized atlas, thus bringing them into register. Another possible future direction for more closely comparing our data with his study would be to obtain the raw data and counts from the Hahn study so they can then be used to more directly compare distributions across animals and generate maps that show more precise trends of consistency across cases.

IV.2. Technical and methodological considerations

IV.2.1. Mapping

The size and scope of the present study necessitated the input of multiple students who participated in the generation of the peptide maps presented here. While beneficial, this multi-user mapping effort requires careful considerations, since having a team working on generating maps introduces additional sources of variability, including possible variance between students. For our study, major sources of variability can be traced to two transformations of data: the first of these is the transformation of the raw data from the photomicrographs of the tissue sections and the second of these is the translation of data from the photomicrographs to the corresponding Swanson atlas. As explained in the Methods section, the plotting of fibers and somata was performed by superimposing the Nissl parcellation file and photomicrographs of the DAB stain. Ellipses and hand-drawn lines were then placed in a separate data layer overlaid on the data layer holding the DAB photomicrograph. This arrangement allowed each student to have his or her own interpretation of the amount of representation that should be given to each neuropeptide. This leads to a range of representations between students, which we observed to become apparent in one of two ways: some would be overly detailed and preferred a more one-to-one representation of every single fiber/mark on the photomicrograph, while others would take a more abstract approach, being more mindful of representing the trends that were present rather than creating a one-to-one representation. To mitigate the variance introduced by these different interpretations, student maps were continuously checked by more senior graduate students. Upon completion of mapping, students were provided feedback, with the goal of helping them improve their representation of the data. It must be mentioned, however, that this was of serious concern only with the representation of fibers. This is due to the further refinement of somata counts and placements that

was performed with the use of a microscope at ×100 magnification, when the putative apposition checks were taking place. During these checks, all erroneously marked somata were removed and any somata which were not marked were then added during this process. This process provided us with more certainty about the representations of somata in this study.

Similarly, when examining the translation of data to the Swanson atlas, there is a similar introduction of interpretive variability. The effects of these are not of major concern when considering intra-regional representation, because of the method used to transfer these data. Specially, when moving ellipses and lines from the photomicrograph to the Swanson atlas templates, all of these elements within one sub-region are group-selected using the *Lasso Tool* in Adobe Illustrator and copied and pasted onto the atlas template. These are then transformed as one unit to preserve the trends observed in the photomicrographs of the tissue.

In order to account for these variations, we have devised a rubric that will assess the mapping of all those who have participated in the generation of these maps. A blind study with a set of controls to score the two transformation steps of data will be performed with the help of three experts. These experts are individuals who have had much experience performing the techniques of immunohistochemistry and mapping and did not participate in generating any of the data presented here. These control studies are separated into three categories: control tests for the quality of immunocytochemical stain and photomicrography, for raw mapping, and for translation of the data to Swanson atlas maps. Cases will be separated into pairs (A and B) that will allow for assessment of these three categories. Rubrics will be provided to each scorer which will give a score ranging between 1 – 3 with: 1 = no variability between the pair, 2 = some discrepancies between the pair, and 3 = variability between the pair is very high. These scores will help validate the interpretations of the individuals who were involved in the staining of the tissues and in the mapping of the

neuropeptides presented in this study, thus providing a measure of reliability to the mapping process and ensuing its reproducibility. This is currently underay and is another near-term future direction that will be realized once these data are submitted for publication.

IV.2.2. Cell counts and putative appositions

Cell counts were performed on data that had already undergone translation to the Swanson atlas. With the use of the *Lasso* tool in Adobe Illustrator, all ellipses within a specific sub-region were highlighted and a readout for the selections was given by the *Document Info* tool. This readout of ellipses is the number that was used for the cell counts reported in this study. Due to the methodology used here, there were some instances where ellipses placed on the border of two sub-regions could be counted for either sub-region; this could lead to a small discrepancy in cell counts between regions. Once these numbers were proofread, the processed averages and percentages by sub-region and total level were performed with the use of Excel.

Putative apposition analysis adds yet another area for some interpretive variation between individuals involved in this process. To minimize this, criteria for the identification of appositions were generated based on previously published studies that reported putative-apposition analysis using bright-field microscopy as a visualization method. The use of these criteria facilitates discussion between those who performed putative apposition analysis, which in turn allows for consensus of what types of somata would be considered to contain putative appositions and which would be disregarded. Each student participating in this process practiced under the supervision of a graduate student who confirmed any judgments that were considered difficult by the student. This allowed for discussion and consensus among those performing the studies. However, it must be acknowledged that this does not remove variability completely. The consistency of areas

containing putative appositions gives us some degree of confidence that there was a general agreement among all those who performed this analysis.

It must also be acknowledged that the use of bright-field microscopy is limited when it comes to the magnification that can be achieved. This means that the putative appositions that we are able to observe may not be synaptic in nature. In order to further explore if these putative appositions are synaptic, we would have to perform electron microscopy in order to confirm whether the identified appositions formed true synapses. This is yet another future direction that is being addressed currently and will be included once these data are submitted for publication. The maps we have generated here have been provided to a collaborator, who will be providing us with electron microscopy photomicrographs that will be informed by the patterns that we have observed in this study.

There is also a time-of-day effect that must be taken into consideration when analyzing the distributions of each of these neuropeptides, especially with αMSH, which has been documented to have distinct diurnal patterns (O'Donohue et al 1979). In our study, this variable was accounted for, since all animals were perfused at 3–5 hours after the start of their light phase.

IV.3. Concluding statement

The goal of this study was to provide a comprehensive overview of the cytoarchitectural distributions for H/O-ir and MCH-ir cell populations with respect to αMSH-ir fibers. In performing this type of identification and localization, one can analyze areas that contain regions of higher probability for finding putative appositions between neuropeptidergic systems. These are referred to here as "probable synaptic interaction zones" (PSIZs), which our laboratory will be generating maps for as we expand the work presented here. Even though the presence of putative

appositions from αMSH-ir axonal fibers onto H/O- and MCH-ir cell bodies has been reported previously (Elias et al. 1998; Sakurai et al., 2005), we have provided high-spatial resolution maps which are based on a common neuroanatomical framework (the Swanson atlas), which is something that previous studies had not provided. Additionally, we were able to perform quantification of these interactions and analyze their spatial distributions across the levels sampled here. While MCH- and H/O-ir cell bodies were also found at more caudal levels, which we did not map, detailing all of their distributions was outside the narrow scope of the present study. Overall, the maps that were generated here will facilitate further exploration of interactions between (presumed to be primarily ARH-originating) αMSH-ir fibers with H/O-ir and MCH-ir neuropeptidergic populations of the medial and lateral zones of the hypothalamus. Investigation using functional techniques that require targeting of specific neuronal populations will benefit from the maps generated here. Moreover, the datasets presented provide novel and innovative anatomical data for the anterior and tuberal divisions of the hypothalamus.

Literature Cited

1. Bird, D. J., Baker, B. I., Eberle, A., & Swann, R. W. (1990). The biosynthesis of melanin-concentrating hormone in a fish. *Journal of Neuroendocrinology*, *2*(3), 309–315.

2. Bittencourt, J. C., Presse, F., Arias, C., Peto, C., Vaughan, J., Nahon, J. L., ... & Sawchenko, P. E. (1992). The melanin-concentrating hormone system of the rat brain: an immuno-and hybridization histochemical characterization. *The Journal of Comparative Neurology*, *319*(2), 218–245.

3. Bittencourt, J., & Celis, M. E. (2008). Anatomy, function and regulation of neuropeptide EI (NEI). *Peptides*, *29*(8), 1441–1450.

4. Borgland, S. L., Taha, S. A., Sarti, F., Fields, H. L., & Bonci, A. (2006). Orexin A in the VTA is critical for the induction of synaptic plasticity and behavioral sensitization to cocaine. *Neuron*, *49*(4), 589–601.

5. Chrétien, M., & Mbikay, M. (2016). 60 years of POMC: from the prohormone theory to pro-opiomelanocortin and to proprotein convertases (PCSK1 to PCSK9). *Journal of Molecular Endocrinology*, *56*(4), T49–T62.

6. Cone, R. D. (2005). Anatomy and regulation of the central melanocortin system. *Nature Neuroscience*, *8*(5), 571–578.

7. Dampney, R. A. (2011). The hypothalamus and autonomic regulation: an overview. In *Central regulation of autonomic functions* (I. Llewellyn-Smith, ed.), pp. 47–61. Oxford: Oxford University Press.

8. De Lecea, L., Kilduff, T. S., Peyron, C., Gao, X. B., Foye, P. E., Danielson, P. E., ... & Frankel, W. N. (1998). The hypocretins: hypothalamus-specific peptides with neuroexcitatory activity. *Proceedings of the National Academy of Sciences of the United States of America*, *95*(1), 322–327.

9. Department of Biochemistry and Molecular Biophysics Thomas Jessell, Siegelbaum, S., & Hudspeth, A. J. (2000). *Principles of neural science* (Vol. 4, pp. 1227–1246). E. R. Kandel, J. H. Schwartz, & T. M. Jessell (Eds.). New York: McGraw-Hill.

10. Elias, C. F., Saper, C. B., Maratos-Flier, E., Tritos, N. A., Lee, C., Kelly, J., ... & Sakurai, T. (1998). Chemically defined projections linking the mediobasal hypothalamus and the lateral hypothalamic area. *The Journal of Comparative Neurology*, *402*(4), 442–459.

11. Estabrooke, I. V., McCarthy, M. T., Ko, E., Chou, T. C., Chemelli, R. M., Yanagisawa, M., ... & Scammell, T. E. (2001). Fos expression in orexin neurons varies with behavioral state. *The Journal of Neuroscience*, *21*(5), 1656–1662.

12. Guy, J., Vaudry, H., & Pelletier, G. (1982). Further studies on the identification of neurons containing immunoreactive alpha-melanocyte-stimulating hormone (α-MSH) in the rat brain. *Brain Research*, *239*(1), 265–270.

13. Hahn, J. D. (2010). Comparison of melanin-concentrating hormone and hypocretin/orexin peptide expression patterns in a current parceling scheme of the lateral hypothalamic zone. *Neuroscience Letters*, *468*(1), 12–17.

14. Jacobowitz, D. M., & O'Donohue, T. L. (1978). Alpha-Melanocyte stimulating hormone: immunohistochemical identification and mapping in neurons of rat brain. *Proceedings of the National Academy of Sciences of the United States of America*, *75*(12), 6300–6304.

15. Kawauchi, H., Kawazoe, I., Tsubokawa, M., Kishida, M., & Baker, B. I. (1983). Characterization of melanin-concentrating hormone in chum salmon pituitaries. *Nature*, *305*(5932), 321–323.

16. Kiss, J. Z., Cassell, M. D., & Palkovits, M. (1984). Analysis of the ACTH/β-End/α-MSH-immunoreactive afferent input to the hypothalamic paraventricular nucleus of rat. *Brain Research*, *324*(1), 91–99.

17. Krimer, L. S., Jakab, R. L., & Goldman-Rakic, P. S. (1997). Quantitative three-dimensional analysis of the catecholaminergic innervation of identified neurons in the macaque prefrontal cortex. *The Journal of Neuroscience*, *17*(19), 7450–7461.

18. Lambe, E. K., Krimer, L. S., & Goldman-Rakic, P. S. (2000). Differential postnatal development of catecholamine and serotonin inputs to identified neurons in prefrontal cortex of rhesus monkey. *The Journal of Neuroscience*, *20*(23), 8780–8787.

19. Marcus, J. N., Aschkenasi, C. J., Lee, C. E., Chemelli, R. M., Saper, C. B., Yanagisawa, M., & Elmquist, J. K. (2001). Differential expression of orexin receptors 1 and 2 in the rat brain. *The Journal of Comparative Neurology*, *435*(1), 6–25.

20. Nahon, J. L. (2006). The melanocortins and melanin-concentrating hormone in the central regulation of feeding behavior and energy homeostasis. *Comptes Rendus Biologies*, *329*(8), 623–638.

21. Nahon, J. L., Presse, F., Bittencourt, J. C., Sawchenko, P. E., & Vale, W. (1989). The rat melanin-concentrating hormone messenger ribonucleic acid encodes multiple putative neuropeptides coexpressed in the dorsolateral hypothalamus. *Endocrinology*, *125*(4), 2056–2065.

22. Qu, D., Ludwig, D. S., Gammeltoft, S., Piper, M., Pelleymounter, M. A., Cullen, M. J., ... & Maratos-Flier, E. (1996). A role for melanin-concentrating hormone in the central regulation of feeding behaviour. *Nature*, *380*(6571), 243–247.

23. Rao, T. L., Kokare, D. M., Sarkar, S., Khisti, R. T., Chopde, C. T., & Subhedar, N. (2003). GABAergic agents prevent alpha-melanocyte stimulating hormone induced anxiety and anorexia in rats. *Pharmacology, Biochemistry and Behavior*, *76*(3–4), 417–423.

24. Richardson, K. A., & Aston-Jones, G. (2012). Lateral hypothalamic orexin/hypocretin neurons that project to ventral tegmental area are differentially activated with morphine preference. *The Journal of Neuroscience*, *32*(11), 3809–3817.

25. Rossi, M., Choi, S. J., O'shea, D., Miyoshi, T., Ghatei, M. A., & Bloom, S. R. (1997). Melanin-concentrating hormone acutely stimulates feeding, but chronic administration has no effect on body weight. *Endocrinology*, *138*(1), 351–355.

26. Routh, V. H., Hao, L., Santiago, A. M., Sheng, Z., & Zhou, C. (2014). Hypothalamic glucose sensing: making ends meet. *Frontiers in Systems Neuroscience*, *8*, 236.

27. Sakurai, T., Amemiya, A., Ishii, M., Matsuzaki, I., Chemelli, R. M., Tanaka, H., ... & Arch, J. R. (1998). Orexins and orexin receptors: a family of hypothalamic neuropeptides and G protein-coupled receptors that regulate feeding behavior. *Cell*, *92*(4), 573–585.

28. Sakurai, T., Nagata, R., Yamanaka, A., Kawamura, H., Tsujino, N., Muraki, Y., ... & Koyama, Y. (2005). Input of orexin/hypocretin neurons revealed by a genetically encoded tracer in mice. *Neuron*, *46*(2), 297–308.

29. Saper, C. B., & Lowell, B. B. (2014). The hypothalamus. *Current Biology*, *24*(23), R1111–R1116.

30. Sheng, Z., Santiago, A. M., Thomas, M. P., & Routh, V. H. (2014). Metabolic regulation of lateral hypothalamic glucose-inhibited orexin neurons may influence midbrain reward neurocircuitry. *Molecular and Cellular Neuroscience*, *62*, 30–41.

31. Siemens, J., & Kamm, G. B. (2018). Cellular populations and thermosensing mechanisms of the hypothalamic thermoregulatory center. *Pflügers Archiv-European Journal of Physiology*, *470*(5), 809–822.

32. Simerly, R. B. (2015). Organization of the hypothalamus. In, *The rat nervous system* (G. Paxinos, ed.), pp. 267–294. San Diego: Academic Press.

33. Simmons, D. M., & Swanson, L. W. (1993). The Nissl stain. *Neuroscience Protocols*, *50*(12), 1–7.

34. Star, R. A., Rajora, N., Huang, J., Stock, R. C., Catania, A., & Lipton, J. M. (1995). Evidence of autocrine modulation of macrophage nitric oxide synthase by alpha-melanocyte-stimulating hormone. *Proceedings of the National Academy of Sciences of the United States of America*, *92*(17), 8016–8020.

35. Swanson, L. W. (2018). *Brain maps 4.0—Structure of the rat brain*: An open access atlas with global nervous system nomenclature ontology and flatmaps. *The Journal of Comparative Neurology*, *526*(6), 935–943.

36. Swanson, L. W., Sanchez-Watts, G., & Watts, A. G. (2005). Comparison of melanin-concentrating hormone and hypocretin/orexin mRNA expression patterns in a new parceling scheme of the lateral hypothalamic zone. *Neuroscience Letters*, *387*(2), 80–84.

37. Teegala, S. B., Sheng, Z., Salal, M. S., Hirschberg, P. R., Beck, K. D., & Routh, V. H. (2018). Lateral hypothalamic orexin glucose-inhibited neurons may regulate reward-based feeding by modulating glutamate transmission in the ventral tegmental area. *Brain Research*, *1731*:145808.

38. Verret, L., Goutagny, R., Fort, P., Cagnon, L., Salvert, D., Léger, L., ... & Luppi, P. H. (2003). A role of melanin-concentrating hormone producing neurons in the central regulation of paradoxical sleep. *BMC Neuroscience*, *4*(1), 19.

39. Yang, Y. (2011). Structure, function and regulation of the melanocortin receptors. *European journal of pharmacology*, *660*(1), 125-130.

40. Zséli, G., Vida, B., Martinez, A., Lechan, R. M., Khan, A. M., & Fekete, C. (2016). Elucidation of the anatomy of a satiety network: Focus on connectivity of the parabrachial nucleus in the adult rat. *The Journal of Comparative Neurology*, *524*(14), 2803–2827.

Appendix: List of Neuroanatomical Abbreviations

AHN	anterior hypothalamic nucleus
AHNa	anterior hypothalamic nucleus anterior part
AHNc	anterior hypothalamic nucleus central part
AHNd	anterior hypothalamic nucleus dorsal part
AHNp	anterior hypothalamic nucleus posterior part
ARH	arcuate hypothalamic nucleus
DMH	dorsomedial hypothalamic nucleus
DMHa	dorsomedial hypothalamic nucleus anterior part
DMHp	dorsomedial hypothalamic nucleus posterior part
DMHv	dorsomedial hypothalamic nucleus ventral part
l	internuclear hypothalamic area
LHA	lateral hypothalamic area
LHAad	lateral hypothalamic area anterior group anterior region dorsal zone
LHAai	lateral hypothalamic area anterior group anterior region intermediate zone
LHAav	lateral hypothalamic area anterior group anterior region ventral zone
LHAd	lateral hypothalamic area middle group lateral tier dorsal region
LHAjd	lateral hypothalamic area middle group medial tier juxtadorsomedial region
LHAjp	lateral hypothalamic area middle group medial tier juxtaparaventricular region
LHAjvd	lateral hypothalamic area middle group medial tier juxtaventromedial region dorsal zone
LHAjvv	lateral hypothalamic area middle group medial tier juxtaventromedial region ventral zone
LHAma	lateral hypothalamic area middle group lateral tier ventral region magnocellular nucleus

LHApc lateral hypothalamic area middle group lateral tier ventral region parvicellular region

LHAs lateral hypothalamic area middle group perifornical tier suprafornical region

LHAsfa lateral hypothalamic area middle group perifornical tier subfornical region anterior zone

LHAsfp lateral hypothalamic area middle group perifornical tier subfornical region posterior zone

LHAvl lateral hypothalamic area middle group lateral tier ventral region lateral zone

LHAvm lateral hypothalamic area middle group lateral tier ventral region medial zone

PH posterior hypothalamic nucleus

PVa periventricular hypothalamic nucleus anterior part

PVH paraventricular hypothalamic nucleus

PVHdp paraventricular hypothalamic nucleus descending division dorsal parvicellular part

PVHf paraventricular hypothalamic nucleus descending division forniceal part

PVHlp paraventricular hypothalamic nucleus descending division lateral parvicellular part

PVHmpd paraventricular hypothalamic nucleus parvicellular division medial parvicellular part dorsal zone

PVHmpdl paraventricular hypothalamic nucleus parvicellular division medial parvicellular part dorsal zone lateral wing

PVHmpv paraventricular hypothalamic nucleus descending division medial parvicellular part ventral zone

PVHpml paraventricular hypothalamic nucleus magnocellular division posterior magnocellular part lateral zone

PVHpmm paraventricular hypothalamic nucleus magnocellular division posterior magnocellular part medial zone

PVHpv paraventricular hypothalamic nucleus parvicellular division periventricular part

PVi periventricular hypothalamic nucleus anterior part intermediate zone

RCH	lateral hypothalamic area anterior group retrochiasmatic area
SBPV	subparaventricular zone
SOp	supraoptic nucleus principal part
SOr	supraoptic nucleus retrochiasmatic part
TUi	lateral hypothalamic area middle group lateral tier tuberal nucleus intermediate part
TUl	lateral hypothalamic area middle group lateral tier tuberal nucleus lateral part
TUsv	lateral hypothalamic area middle group lateral tier tuberal nucleus subventromedial part
TUte	lateral hypothalamic area middle group lateral tier tuberal nucleus terete part
VMH	ventromedial hypothalamic nucleus
VMHa	ventromedial hypothalamic nucleus anterior part
VMHc	ventromedial hypothalamic nucleus central part
VMHdm	ventromedial hypothalamic nucleus dorsomedial part
VMHvl	ventromedial hypothalamic nucleus ventrolateral part
ZI	zona incerta
ZIda	zona incerta dopaminergic group

Vita

Vanessa Navarro was born in Riverside, California. She was raised by her mother Clara Navarro in Cd. Juarez, Chihuahua, alongside her sister Claudia Navarro. She and her family moved to the city of El Paso, Texas, in 2008, and she graduated from Coronado High School in 2011. During the fall she enrolled in the University of Texas at El Paso, where she later graduated with her Bachelor of Science degree in Biochemistry in spring 2017. While as an undergraduate student, she joined Dr. Karine Fénelon's laboratory, where she focused on characterizing the effects of antioxidants on firing properties of neurons using field potential recordings. After she graduated, she decided to start her graduate studies by joining the Master's program in Dr. Fénelon's laboratory. After two years, she transferred to Dr. Arshad Khan's systems neuroscience laboratory, where she finished her Master of Science degree in Biological Sciences with an investigation of the possible interactions between feeding-related neuropeptides in the hypothalamus. As a Master's student, she worked as a teaching assistant for Human Anatomy and Physiology II, General Biology, and the PERSIST Brain Mapping and Connectomics teaching laboratory, where undergraduate freshmen have the opportunity to be part of a research laboratory and learn how to conduct graduate-level research about the brain.